THE ASTROPHYSICAL JOURNAL, 444:376–395, 1995 May 1

THE FU ORIONIS OUTBURST AS A THERMAL ACCRETION EVENT: OBSERVATIONAL CONSTRAINTS FOR PROTOSTELLAR DISK MODELS[1]

K. R. BELL[2] AND D. N. C. LIN
University of California Observatories/Lick Observatory, University of California, Santa Cruz, CA 95064;
bell@cosmic.arc.nasa.gov, lin@lick.ucsc.edu

AND

L. W. HARTMANN AND S. J. KENYON
Harvard-Smithsonian Center for Astrophysics, 60 Garden Street, Cambridge, MA 02138;
hartmann@cfa.harvard.edu, kenyon@cfa.harvard.edu
Received 1994 May 13; accepted 1994 November 8

ABSTRACT

The results of the time-dependent disk models developed in Bell & Lin are compared with observed properties of FU Orionis variables. Specific models are fit to the light curves of FU Ori, V1515 Cyg, and V1057 Cyg. The slow risetime of V1515 Cyg can be matched by a self-regulated outburst model. The rapid risetimes of FU Ori and V1057 Cyg can be fitted with the application of modest perturbations to the disk surface density. Model disks display spectral features characteristic of observed objects. The color evolution of V1057 Cyg is naturally explained if mass flux drops in the inner disk ($r < \frac{1}{4}$ AU) while remaining steady in the outer disk. The decrease in optical line width (rotational velocity) observed during the decay of V1057 Cyg may be accounted for by an outward-propagating ionization front. We predict that before final decay to the quiescent phase, short-wavelength line widths ($\lambda < 1.5$ μm) will again increase. It is suggested that FU Orionis outbursts primarily occur to systems during the embedded phase with ages less than several times 10^5 yr.

Subject headings: accretion, accretion disks — stars: evolution — stars: pre–main-sequence — stars: variables: other (FU Orionis)

1. INTRODUCTION

The FU Orionis objects are thought to be young, solar-type stars surrounded by rapidly accreting disks (Hartmann, Kenyon, & Hartigan 1993, and references therein). During outburst, these objects brighten optically by five magnitudes or more, implying an increase in accretion rate through the disk from $\sim 10^{-7}$ to $\sim 10^{-4}$ $M_\odot$ yr^{-1} over timescales of 1–20 yr. FU Ori outbursts are long-lived, lasting for 30–100 yr which implies the accretion of up to 10^{-2} $M_\odot$, a minimum mass solar nebula, in only a century (Hartmann et al. 1993). Event statistics suggest that a typical solar-type star undergoes 10–100 such outbursts in its pre–main-sequence lifetime (Herbig 1989).

Two primary explanations for the mechanism behind FU Ori outbursts have been advanced. Perturbation of the disk by a passing binary companion may produce episodic accretion events (Bonnell & Bastien 1992), but it is not clear whether such a mechanism can account for the required event frequency (e.g., Duquennoy & Mayor 1991). Also, no Fuor has shown any displacement in velocity greater than 5 km s^{-1} from its associated molecular cloud (Herbig 1977; Hartmann & Kenyon 1987a, b) which provides little evidence for a binary interaction with a companion comparable in mass to the central object. A second promising mechanism for the outburst is a thermal instability of the type suggested to occur in the disks of cataclysmic variables (Hartmann & Kenyon 1985; Lin & Papaloizou 1985), and it is this possibility which has received the most detailed treatment. Lin & Papaloizou (1985) show that thermal instabilities can in principle account for the large outbursts. Clarke, Lin, & Pringle (1990), using as pre-outburst conditions standard T Tauri disk accretion rates of 10^{-7} $M_\odot$ yr^{-1}, found it difficult to maintain outbursts at accretion rates of $\sim 10^{-4}$ $M_\odot$ yr^{-1} for the hundred years suggested by observed outbursts. They were able to produce a model outburst lasting ~ 30 yr, but only with the imposition of the extremely large "perturbation" in surface density of $\Delta\Sigma/\Sigma = 50$. The model is also unable to account for the repetition of events in a given source.

With great improvements in infrared detection techniques, it has become increasingly clear that FU Ori objects are generally embedded in opaque, dusty clouds (Herbig 1977; Goodrich 1987; Kenyon et al. 1993b). Even optically visible FU Ori objects like V1057 Cyg and V1515 Cyg exhibit far-infared emission which can naturally be explained by an opaque, circumstellar envelope (Kenyon & Hartmann 1991; hereafter KH 91). KH 91 present spectral fits which suggest that FU Ori objects (hereafter "Fuors") are surrounded by close dusty envelopes consistent with material falling onto the outer disk ($\gtrsim 5$ AU) at a rate of $\sim 5 \times 10^{-6}$ $M_\odot$ yr^{-1}. In addition, Adams, Lada, & Shu (1987) suggest that the FU Ori object L1551 IRS 5 possesses an infalling envelope with a mass accretion rate of 7×10^{-6} $M_\odot$ yr^{-1}. Further recent studies (e.g., Kenyon, Calvet, & Hartmann 1993a) suggest that infall rates of $(1–10) \times 10^{-6}$ $M_\odot$ yr^{-1} are common for embedded protostars. Such continuous infall replenishes disk material accreted during the FU Ori outburst allowing eruptions to recur on timescales of several thousand years. These infall rates are expected during the earliest phases of star formation.

The addition of mass to the outer disk at these high rates implies very different initial conditions than have previously been explored in thermal instability models. Kawazoe & Mineshige (1993) show that adding mass to protostellar disks at

[1] Lick Observatory Bulletin No. 1291.
[2] Now at NASA Ames Research Center, MS 245-3, Moffett Field, CA 94035.

$10^{-5}\ M_\odot\ \mathrm{yr}^{-1}$ can in principle lead to FU Ori–like outbursts. Using detailed, time-dependent disk calculations, which include a one-dimensional treatment of vertical convective energy transport, Bell & Lin (1994, hereafter BL 94) show that, independent of reasonable values of the viscous efficiency (α), the addition of mass at a rate greater than the critical rate of $\dot{M}_{\rm crit} = 5 \times 10^{-7}\ M_\odot\ \mathrm{yr}^{-1}$ is sufficient to trigger thermal disk instabilities with properties very like those inferred for FU Ori objects. In particular, long-duration outbursts (~ 100 yr) result without the need for perturbation and repeat on statistically reasonable timescales (~ 1000 yr). This extremely encouraging result is limited by the necessity of appealing to the ad hoc α viscosity (Shakura & Sunyaev 1973). Such detailed models, however, make *predictions* which can be compared with observations, so that even in the absence of a detailed understanding of the viscosity, it is possible to make specific tests of the thermal instability model.

In this paper the Bell & Lin disk-outburst models are used to explore observational tests of the thermal instability theory in application to three specific objects: FU Ori, V1515 Cyg, and V1057 Cyg. The self-regulated BL 94 outburst models are used to explain the relatively slow risetime of V1515 Cyg (~ 20 yr), but have difficulty explaining the rapid risetimes (~ 1 yr) of FU Ori and V1057 Cyg. We find the application of small surface density perturbations to supercritical disks results in prematurely triggered outbursts which exhibit the observed rapid risetimes. *Based solely on fits to B magnitude light curves*, specific model parameters are chosen for each of the three program objects suggesting physical constraints on disk properties. The time-dependent appearance of disk outburst models is then compared to observations of evolving colors, line widths, and spectral energy distributions.

In this contribution we also specifically address two of the principal objections raised to the accretion-event scenario as an explanation of FU Orionis outbursts. (1) It has been noted that there has been too little decline in the 2–5 μm region of V1057 Cyg to be explained by a series of constant mass flux disk models with decreasing accretion rates (Kenyon, Hartmann, & Hewett 1988, hereafter KHH 88; Simon & Joyce 1988). In particular KHH 88 find *no* variation in the M band (4.8 μm) during the early decay from peak light while the U band decreased in brightness by 4 mag. (2) If the decline is modeled as a sequence of steady disk models with decreasing mass flux, rotational line widths at a given wavelength should come from successively smaller disk radii and velocities should therefore increase with time. That the line widths of V1057 Cyg are observed to *decrease* after outburst is regarded as a "clear conflict" with the accretion-disk outburst model (Herbig 1989). The thermal outburst model provides simple explanations for these apparent discrepancies.

Observations of the three best-studied FU Ori objects—FU Ori, V1515 Cyg, and V1057 Cyg—with emphasis on time-dependent phenomena which cannot be explained by constant mass flux models are summarized in § 2. In § 3, the Bell & Lin self-regulated models are briefly reviewed, and our method of perturbing the surface density to produce rapid-risetime outbursts is introduced. In § 4, models are developed which fit the light curves of each of the three program Fuors. Implications of the time-dependent models are then investigated by comparing "observations" of the models with data presented in § 2. The detailed evolution of model magnitudes, colors, absorption line widths, and spectral energy distributions are specifically discussed. Also in this section, the possible statistical identification of FU Ori objects in the quiescent phase between outbursts is discussed, and suggestions are made for the identification of particular quiescent outbursters. Model implications and limitations are discussed in § 5, and a summary is given in § 6.

2. OBSERVATIONAL SUMMARY

In outburst, Fuors have distinctive characteristics unique among young stellar objects, many of which in recent years have found explanation in a system in which the surrounding protostellar disk far outshines the central star (Hartmann & Kenyon 1985, 1987a). Broader-than-blackbody spectra have been modeled as arising from a luminous constant-mass-flux disk actively accreting at rates of order $10^{-4}\ M_\odot\ \mathrm{yr}^{-1}$ (KHH 88). This scenario, in which longer wavelengths are generated at larger disk radii where temperatures are cooler, naturally explains one of the earliest noted peculiarities about FU Ori spectra which is that spectral types are systematically later at longer wavelengths (Herbig 1977). At peak light, for example, V1057 Cyg is estimated to have a spectral type of early F at 4000 Å, late F at 5000 Å, and early G at 6000 Å (KHH 88).

High-resolution Fuor spectra typically show low-gravity absorption lines (quite unlike T Tauri high-gravity emission lines) thought to arise in the atmosphere of a thermally stratified, self-luminous accretion disk (Hartmann & Kenyon 1985; Carr 1988). Further these absorption lines show a characteristic doubling which is strongest at short wavelengths. The observation that this doubling increases at short wavelengths in a manner consistent with the expected increase in Keplerian velocity from inner, hotter radii (Welty et al. 1990) is currently one of the strongest arguments in support of the idea of FU Ori objects as luminous, actively accreting disks.

This simple model in which FU Orionis outbursters are considered to be high accretion rate constant-mass-flux disks has been a very powerful tool in the interpretation of observations of FU Orionis systems. Such models, however, make no attempt to explain the mechanism by which the disk makes the transition from some (presumably low-mass flux) quiescent state to the high-mass-flux outburst state. Further, certain observations (particularly time-dependent observations) cannot be addressed with this quasi-steady-state model. In the rest of this section, observed properties of the three best studied Fuors—FU Ori, V1515 Cyg, and V1057 Cyg (which we hereafter refer to as our program objects)—are summarized with emphasis on *time-dependent* phenomena which cannot be explained by constant-mass-flux models.

2.1. *Light Curves*

In our modeling of the outbursts, the *shape* and *peak magnitude* of program object light curves are used to constrain disk properties. Light curves of the three Fuors with detailed observations show remarkable variety. Figure 1 shows the combined optical and photographic light curves: $B(t)$ ($B \sim 4400$ Å) for the three program objects. Observed magnitudes are given on the left axis, and derived absolute magnitudes are estimated on the right axis (see Table 1; note that, in addition to considerable observational scatter, uncertainties in extinction lead to uncertainties in M_B of about ± 0.5). All three objects exhibit similar large magnitude outbursts. All three objects have similar current magnitudes $M_B \sim 0$. Two objects—FU Ori and V1057 Cyg—have rapid risetimes of about a year and reach very bright peak absolute magnitudes of $M_B \simeq -2$ before fading to their current luminosities. In

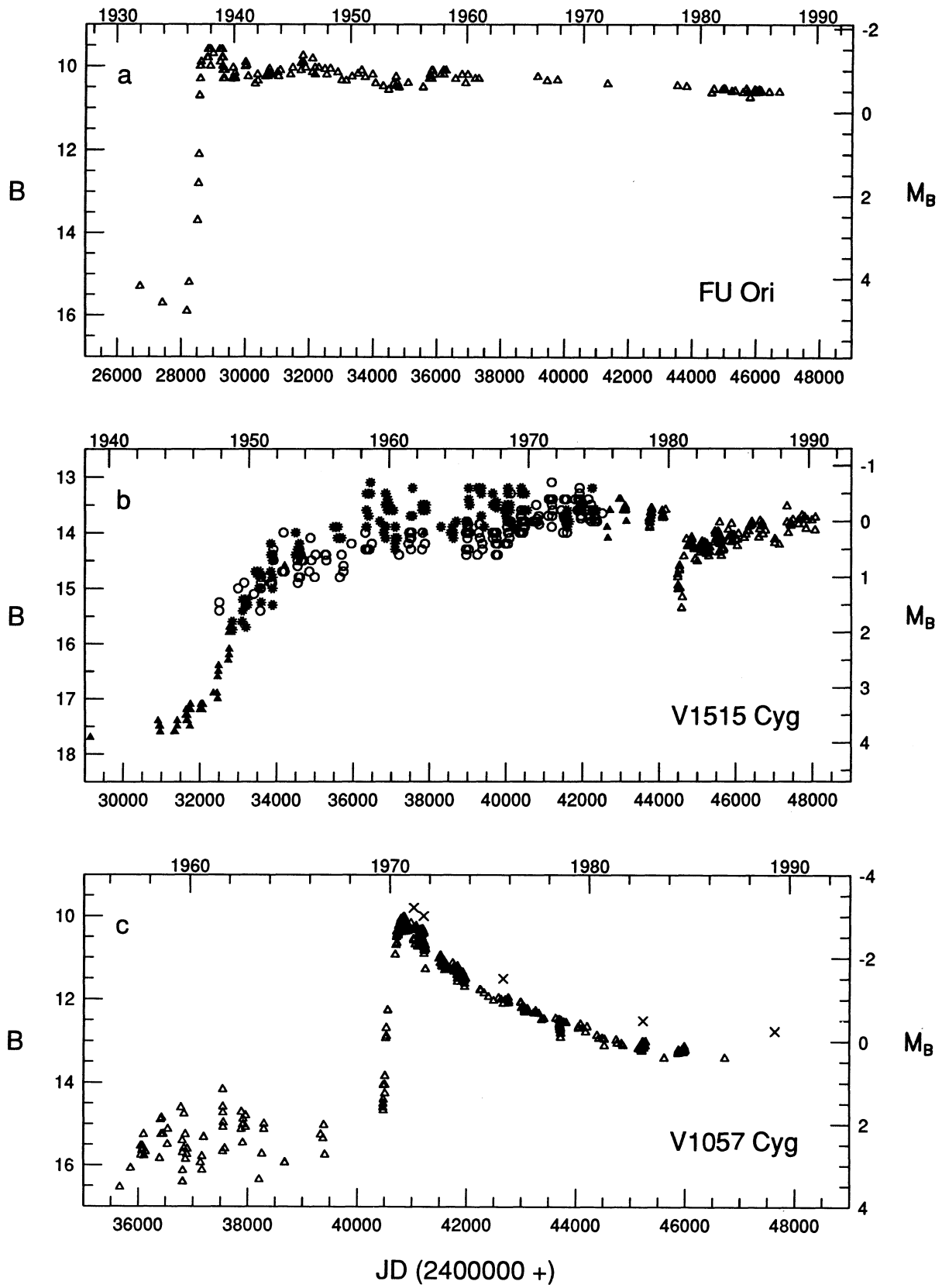

FIG. 1.—Combined photographic and *B* light curves for program Fuors with estimated M_B on right axis. (*a*) FU Ori; compiled by Hartmann et al. (1993). (*b*) V1515 Cyg. *Filled triangles*: Gottlieb & Liller (1978); *other symbols*: compiled by Kenyon et al. (1991); note discrepancy between open circles (Hoffleit) and asterisks (Wenzel). (*c*) V1057 Cyg; compiled by Kenyon & Hartmann (1991). Crosses indicate epochs of SEDs shown in Fig. 3.

TABLE 1

OBSERVATIONALLY DERIVED PARAMETERS OF PROGRAM FUORS

Parameter	FU Ori		V1515 Cyg		V1057 Cyg		References
Distance (pc)	500		1050		600		...
A_V	2.0 ± 0.3		2.8 ± 0.3		3.1 ± 0.3		3–4, 5, 2
R_V	3.5		3.1		3.1		4, 6, 6
Inclination	25°–70°		...		$<30°$		4
$B - M_B$[a]	11.1		13.8		13.0		...
	B	M_B	B	M_B	B	M_B	...
Preoutburst[b]	15–16	3.9–4.9	17.5	3.7	15.5–16.5	2.5–3.5	2, 1, 2
Peak light	10	−1.1	13.5	−0.3	10.5	−2.5	2
T_{max}(K)[c]	7200 ± 400		≈ 7000		6600 ± 400		4, 5, 4
$M_* \dot{M}$ ($M_\odot^2$ yr^{-1})[c,d]	$(0.5–4) \times 10^{-4}$		...		$(0.5–3) \times 10^{-4}$		4

[a] Adopted combined extinction and distance correction: $B - M_B = 5 \times \log_{10}(d/10\ \mathrm{pc}) + A_B$ where $A_B = A_V + E(B-V) = A_V \times (1 + 1/R_V)$. Note that quoted uncertainties in A_V translate into uncertainties in A_B of ± 0.4.

[b] Range indicates variability.

[c] Fits to current spectral energy distributions.

[d] Note that Kenyon et al. 1988 assume $M_* = 0.5\ M_\odot$.

REFERENCES.—(1) Gottlieb & Liller 1978; (2) Herbig 1977; (3) Kenyon & Hartmann 1991; (4) Kenyon et al. 1988; (5) Kenyon et al. 1991; (6) Savage & Mathis 1979.

contrast, V1515 Cyg, after an initially rapid brightening to $M_B \sim 2$, has a much slower rise to a peak light very close to its current value. (The 1980 drop in magnitude is thought to be the result of a dust condensation event in the wind; Kenyon, Hartmann, & Kolotilov 1991; hereafter KHK 91.) The three objects show a remarkable variety of risetime light curve shapes, but all have similar slow declines. Note also that the three objects have *nearly identical preoutburst absolute magnitude* $M_B = 3$–4 (Herbig 1977).

Light curves at other wavelengths from the optical through the near-infrared show that changes in magnitude are systematically greatest at short wavelengths (KH 91). For V1057 Cyg, since peak light $\Delta U \sim 4$ (0.36 μm) while $\Delta M \sim 0$ (4.8 μm). A preoutburst estimate of the R-band magnitude for V1057 Cyg of $R \sim 12.7$ (0.7 μm; Haro 1972) suggests that this trend was also characteristic of the rise to peak light: $\Delta B \approx -5$ while $\Delta R \approx -3$. This trend, however, does not seem to continue to the mid- and far-infrared; decay in the 10–20 μm region closely mimics decay at the shortest wavelengths and can be modeled as the reprocessing of inner disk photons in a flattened, infalling envelope (KH 91). It will be shown that the tendency for magnitude changes to be greatest at short wavelengths is characteristic of the radially restricted, thermal-outburst models.

2.2. *V1057 Cyg*

The most detailed spectral information available comes from the recent outburst of V1057 Cyg which since peak light in 1969 has shown an uncharacteristically rapid decline. V1057 Cyg is also the only object with a preoutburst spectrum from which hints about FU Ori progenitors can be derived. Although of low dispersion, the spectrum shows typical T Tauri–type emission lines (Herbig 1977). It is this evidence which suggests most strongly that the class of objects subject to FU Orionis–type outbursts is not remarkably different from the class of typical T Tauri objects. A notable feature of this early spectrum is that, because there were no absorption lines from which a spectral type could be determined, the preoutburst V1057 Cyg was classified a "continuum" source. Although continuum sources are not unheard of among T Tauri objects, they are not common (8/72 in Beckwith et al. 1990).

As well as being a function of wavelength at any one time, the spectral type of V1057 Cyg at one wavelength has been observed to change over time. At peak light the optical spectral type was that of an A-F supergiant. During the decay phase it cooled to that of an early-G supergiant (Herbig 1977; KHH 88; KH 91). This variation in spectral type suggests that the dropping luminosity is not due merely to changing obscuration, but signifies real changes in the properties of the underlying object.

Figure 2 shows the $B-V$ and $R-I$ color evolution of V1057 Cyg since 1969 (again observed colors are on the left axis while absolute colors estimated from corrections in Table 1 are on the right axis). Before outburst, V1057 Cyg was noted to be "rather red" (Herbig 1977) and an estimate by Haro (1972) suggests that in 1965, $R-I \sim 1.8$. This estimate appears as a filled square along with more recent $R-I$ colors in Figure 2. Color evolution is summarized as follows. Throughout evolution $B-V > R-I$. During the rise to peak light, the colors decrease, and $B-V$ decreases more than $R-I$ (i.e., changes are again greatest at short wavelengths). Since outburst, colors are consistent with steady increase. It will be seen that not only are these evolutionary features present in model outbursts, but the values of model colors are comparable to the dereddened colors of V1057 Cyg.

2.3. *Line-Width Velocities*

As discussed above, absorption lines in FU Ori objects are thought to arise from the surface of a self-luminous, rotating disk. Different wavelengths probe different temperature regimes and therefore different disk radii. Monitoring of variations in these absorption lines could therefore provide valuable insight into the thermal evolution of the FU Ori disk. Since peak light, optical line widths in V1057 Cyg have decreased from $v \sin i \approx 70$ km s^{-1} in 1973 to ≈ 45 km s^{-1} in 1989 (Herbig 1989). Herbig has argued that this decrease is counter to the disk-outburst model through the following argument. If the declining luminosity of V1057 Cyg since peak light can be modeled as a uniformly cooling accretion disk, the radius at which a given temperature is found should decrease with time. As this radius moves inward, its associated Keplerian rotation rate should increase. The line width at a given wavelength

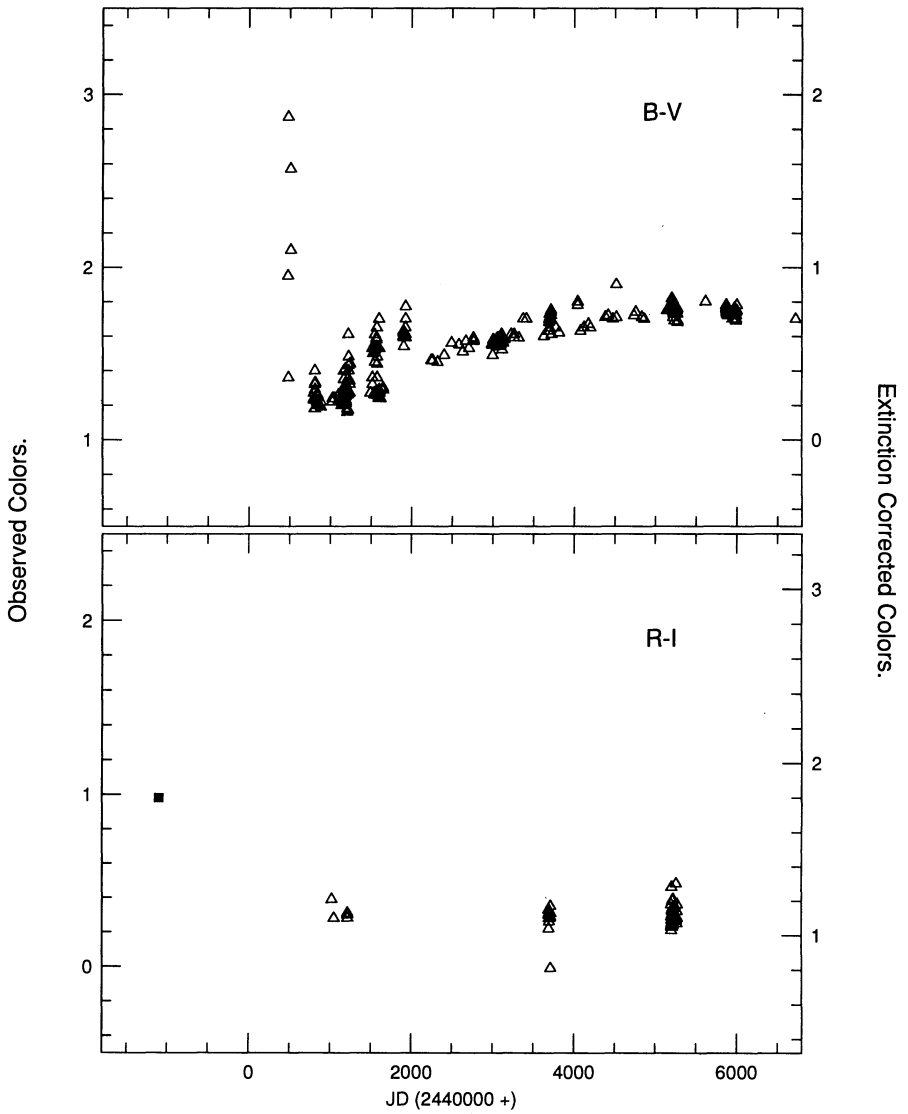

FIG. 2.—V1057 Cyg. Color evolution of $B-V$ and $R-I$. Triangles compiled by Kenyon & Hartmann (1991); filled square represents preoutburst estimate of Haro (1972).

should therefore increase as the object drops in luminosity.[3] That line widths are seen to *decrease* therefore requires additional elaboration of the accretion disk model. It will be seen that decreasing line widths are a natural consequence of the outward propagation of the thermal front during outburst.

2.4. *Spectral Energy Distributions*

Hartmann, Kenyon and collaborators have had a great deal of success modeling the broader than blackbody spectral energy distributions (SEDs) of Fuors as arising from luminous accretion disks by assuming that the mass flux through these disks is the same at all radii (Hartmann & Kenyon 1985; KHH 88; KH 91; KHK 91). Later in this contribution we briefly examine the implications for SEDs of an evolving mass flux distribution.

[3] A similar argument by Hessman et al. (1991) for a small outburst of the FU Ori object Z CMa is questionable, given the evidence that the light variations may be produced by scattered optical light from the luminous infrared companion; Whitney et al. 1993.

Figure 3 shows the dereddened spectral energy distribution of Fuor V1057 Cyg at five epochs during the decline from peak light. Extinction ($A_V \sim 3.5$) is estimated by KHH 88 from the assumption that short-wavelength radiation is well represented by a constant mass flux disk in the fourth epoch (*not* from Table 1). KH 91 note that the fading of the long-wavelength ($\lambda \gtrsim 8$ μm) radiation closely follows the fading of the total luminosity. This additional excess is modeled as arising from the reprocessing of inner-disk photons in a circumstellar envelope with an infalling mass flux of $4 \times 10^{-6}\ M_\odot\ \mathrm{yr}^{-1}$. At short wavelengths ($\lambda \lesssim 1$ μm) radiation is sensitively dependent on both the details of the inner boundary condition and the extinction correction. Our investigation therefore focuses on the slope in the 1–8 μm region which suffers the least contamination from envelope and boundary layer emission. In this region, for a disk with radially constant but temporally decreasing mass flux the slope is expected to be nearly constant (as for dashed lines in Fig. 9*a* below). It can be shown that the observed change in slope during decay from peak light is a

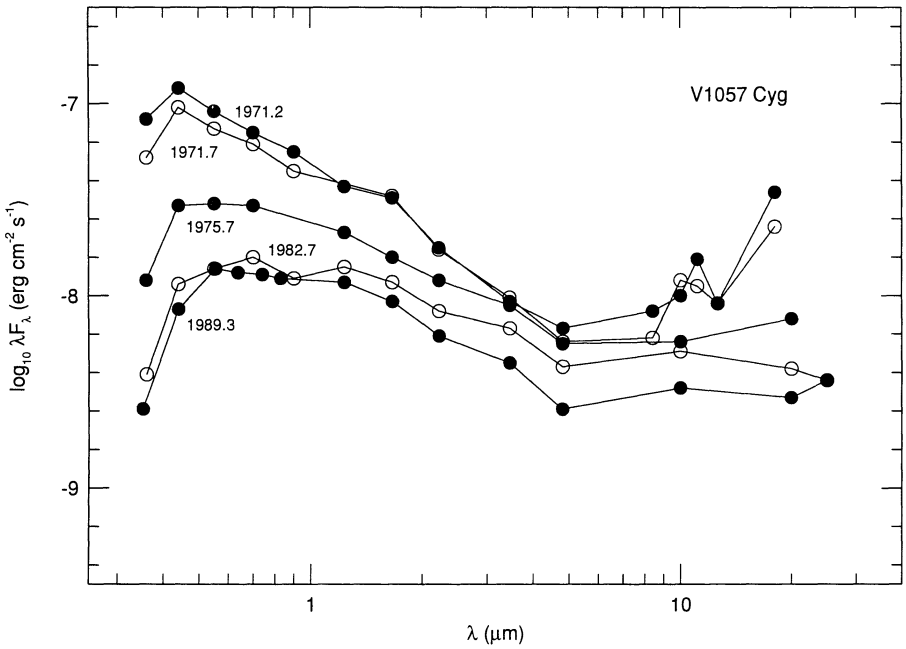

FIG. 3.—Spectral energy distribution of V1057 Cyg at five epochs (Kenyon & Hartmann 1991). Spectra are dereddened with the assumption of a constant mass flux disk in the fourth epoch. The five distributions correspond to JD 2,440,000 + (1027, 1220, 2670, 5214, and 7650); these times are marked with crosses in Fig. 1*c*. Peak light occurs approximately half a year before the first SED at JD 2,440,713 (1969.7).

natural consequence of a disk in which the mass flux is *not* radially constant.

3. METHOD

In this section, the models which will be used in the detailed light curve fitting of the program objects in § 4 are described. The self-regulated BL 94 thermal disk-outburst models which form the numerical basis for the current work are summarized in § 3.1. In these self-regulated outbursts, the ionization front propagates from the inner edge of the disk to the limiting radius $R_{\rm limit}$, producing light curves with timescales comparable to the slow-risetime outburst of V1515 Cyg but too slow to match the more rapid rises of FU Ori and V1057 Cyg. In § 3.2 the temperature distributions of disks with subcritical and supercritical mass fluxes are compared, and it is shown that the latter have a large inner region which hovers on the brink of thermal instability. In § 3.3 the generic propagation of ionization fronts is discussed. It is shown that an inward moving ("outside-in") front will move faster than an outward moving ("inside-out") front and will therefore exhibit a more rapid risetime. In § 3.4 a surface density perturbation is introduced which triggers an inward moving ionization front. In § 3.5 we discuss how the *shape* of a given light curve may be used to estimate the magnitude of the underlying perturbation.

3.1. *Bell & Lin Models*

Bell & Lin (1994) make use of the results of two one-dimensional models to derive disk structure during the outburst cycle. Hydrostatic, atmosphere-type models resolve vertical structure through the nebula and include convective transport of energy (mixing length theory) as well as self-consistently accounting for departures from vertical thermal balance. Results of these models are used principally to calculate the vertical radiative losses (Q^-) for each annulus as a function of central temperature and surface density: $Q^-(T_c, \Sigma)$. The second numerical model is a time-dependent, viscous-diffusion code which calculates the radial evolution of T_c and Σ during the outburst cycle. Local disk heating (Q^+) occurs through in situ viscous dissipation. This process is assumed to far outweigh the effects of irradiation by the central star or inner disk; the effects of reprocessing are ignored. Both models assume axial symmetry and use the same detailed opacities and equation of state. Results assume a 1 $M_\odot$ central object and an inner disk radius of 3 $R_\odot$.

Mass is fed into the outer disk at a constant rate: $\dot{M}_{\rm in}$. If the input mass accretion rate ($\dot{M}_{\rm in}$) lies above a critical mass flux, the disk will heat up to a regime in which the dramatic increase of opacity during the ionization of hydrogen ($\kappa \sim T^{10}$) causes the system to go into outburst. This critical mass flux: $\dot{M}_{\rm crit} \approx 5 \times 10^{-7}\ M_\odot\ {\rm yr}^{-1}$, is found to be *independent of the viscous efficiency* α for the tested range of 10^{-1} to 10^{-4}. The value of $\dot{M}_{\rm crit}$ is somewhat dependent upon the assumed stellar mass and radius: 1 $M_\odot$ and 3 $R_\odot$, respectively (BL 94). During outburst the mass flux through the inner disk greatly exceeds both $\dot{M}_{\rm crit}$ and $\dot{M}_{\rm in}$, and the surface temperature of the disk (6000–8000 K) greatly exceeds that of the star (3000–4000 K). The outburst continues until sufficient mass is drained out of the disk onto the central star for the disk to cool below the recombination temperature of hydrogen. The system then drops back into the low state, and accretion through the inner disk decreases below $\dot{M}_{\rm crit}$.

In a system where the outer disk is fed at a steady rate such that $\dot{M}_{\rm in} = (1\text{–}10) \times 10^{-6}\ M_\odot\ {\rm yr}^{-1} > \dot{M}_{\rm crit}$, model outbursts recur periodically on a timescale governed principally by the low state viscosity. Disks with a viscous efficiency $\alpha = 10^{-4}$ where hydrogen is neutral and 10^{-3} where ionized produce a cycle for which $\gtrsim$100 yr is spent in outburst and $\gtrsim$1000 yr in quiescence. If FU Ori outbursts occur mainly in the embedded phase, which is thought to last a few times 10^5 yr (e.g., Kenyon et al. 1994), these timescales are consistent with observed event statistics.

Throughout the cycle, material is supplied to the outer disk *at a steady rate*, and the outer disk adjusts to this constant mass flux. The smallest radius which can remain stable, $R_{\rm limit}$, is derived in BL 94 and depends on the input mass flux ($\dot{M}_{\rm in}$), the star's mass (M_*), and the surface temperature at which midplane hydrogen begins to ionize (T_d[H]):

$$R_{\rm limit} = 20\, R_\odot \left(\frac{\dot{M}_{\rm in}}{3\times 10^{-6}\, M_\odot\ {\rm yr}^{-1}}\right)^{1/3}\left(\frac{M_*}{M_\odot}\right)^{1/3}\left(\frac{T_d[{\rm H}]}{2000}\right)^{-4/3}. \quad (1)$$

(The value of T_d[H], depends slightly on the radius—cf. Figure 3*a* in BL 94—but not on α.) Note that fronts may travel significantly beyond $R_{\rm limit}$ especially in strongly perturbed systems. Beyond $R_{\rm limjt}$ (in the "outer" disk), mass is stably transported at the rate $\dot{M}_{\rm in}$. Inside $R_{\rm limit}$ (the "inner" disk), the disk cycles between a high-mass flux, outburst state and a low-mass flux, quiescent state. The inner disk is rapidly depleted during outburst and slowly replenished during quiescence. During quiescence, mass accumulates near $R_{\rm limit}$. Outbursts tend to begin near the inner disk edge because it is there that the lowest surface densities are required to ionize hydrogen. The resulting self-regulated outburst is typically an "inside-out" outburst, in which an ionization front is initiated near the inner edge of the disk and propagates out to $R_{\rm limit}$. This outburst cycle has also been used to explain the periodic outbursts of cataclysmic variables (e.g., Lin, Papaloizou, & Faulkner 1985).

During outburst, the disk can be thought of as divided into adjoining disks of differing mass flux: the inner, high-mass-flux region which provides short-wavelength photons and the outer, low-mass-flux region which provides longer-wavelength photons. Each portion of the disk has a vertical scale height which increases with radius: $H \approx 0.3r$ in the inner disk and $H \approx 0.1r$ in the outer disk. The inner disk is therefore not only considerably thicker than the outer disk, but it is bowl-shaped in such a manner that the outer disk is effectively shielded from the intense radiation of the inner disk. Because of this phenomenon and because of the difficulty of computing the mutual reprocessing between two surfaces of constantly changing aspect angle, the effects of reprocessing are not included in our calculation.

3.2. *Subcritical versus Supercritical Disks*

Outbursts may be initiated at any radius of any disk for which the surface density can be elevated above the local critical value: $\Sigma_A(r)$, for a time sufficiently long (several thermal timescales: Lin et al. 1985) to initiate a local thermal runaway. The value of Σ_A is a strongly increasing function of radius (BL 94). In self-regulated outbursts, Σ exceeds Σ_A first at the inner edge of the disk due to the inexorable inward diffusion of matter. Also, outbursts may be artificially triggered in disks through the addition of a perturbation in surface density. How big a perturbation must be to trigger an outburst in a given disk therefore depends sensitively on the initial underlying surface density distribution which in turn depends on the input mass flux.

Model disks can be classified by input mass flux as either "subcritical": $\dot{M}_{\rm in} < \dot{M}_{\rm crit}$, or "supercritical": $\dot{M}_{\rm in} > \dot{M}_{\rm crit}$. In subcritical systems, the surface density and temperature decrease monotonically with radius so the addition of a large perturbation in the surface density is necessary to bring an annulus of the disk to the point of instability. All outbursts in these systems will be triggered because by definition a subcritical disk is not subject to self-regulated outbursts. As Clarke et al. (1990) found with a $10^{-7}\ M_\odot\ {\rm yr}^{-1}$ disk, a subcritical system may require a very large perturbation to trigger thermal outburst.

In supercritical systems, the surface density increases out to the radius $R_{\rm limit}$ given approximately by equation (1) and decreases thereafter. During quiescence, throughout the inner disk ($r < R_{\rm limit}$) the local surface density, Σ, is never far from the critical value for the ionization of hydrogen, Σ_A, and the midplane temperature, T_c, is therefore everywhere close to the ionization temperature of hydrogen. In their inner disks, quiescent supercritical systems are therefore never far from the conditions necessary to initiate the ionization of hydrogen, so perturbations need not be large to trigger an outburst. In supercritical systems, outbursts may be either inside-out (self-regulated or weakly triggered) or outside-in (triggered).

To demonstrate that it is generally easier to trigger outbursts in supercritical systems than in subcritical systems, the radial dependence of the midplane temperature is derived for both cases. In a subcritical or conventional constant mass flux disk $T_c(r)$ is derived by assuming (1) the central density $\rho = \Sigma/2H \approx \Sigma\Omega/2c_s$, (2) the midplane optical depth $\tau_c = \kappa_c \Sigma/2 \gg 1$, (3) the central opacity $\kappa_c = \kappa_i \rho^a T_c^b$ (as in the Appendix of BL 94), and (4) the standard radiative relation $T_{\rm eff}^4 \propto T_c^4/\tau_c$. Solving for $T_c(r)$ using the equation of vertical thermal balance: $Q^- = Q^+$, the radial dependence of the central temperature in a subcritical disk can be shown to be

$$\frac{d\ln T_c}{d\ln r} = -\left\{\frac{9+6a}{10+3a-2b}\right\}. \quad (2)$$

An opacity appropriate for temperatures in the several thousand degree range before H-opacity becomes important is given by $a = \frac{2}{3}$, $b = 3$ (BL 94). These numbers when applied to equation (2) show that the temperature in this regime falls steeply with radius: $T_c \sim r^{-2.2}$. Even if the innermost annulus is on the brink of instability, for a subcritical disk the perturbation required to trigger outburst therefore grows rapidly with radius. In contrast, during quiescence in supercritical disks, $T_c(r)$ interior to $R_{\rm limit}$ is essentially independent of radius, $T_c \sim r^0$ (BL 94), so the entire inner disk hovers on the brink of hydrogen ionization, and outbursts are easy to trigger at any radius within $R_{\rm limit}$ of the central object.

3.3. *Inside-Out versus Outside-In*

Because the increasing optical brightness of the system during the onset of outbursts is principally governed by the changing *area* of the portion of disk in the thermal high state, the rise time is determined by the propagation of the ionization fronts through the inner disk. As background for our discussion of light curve fitting, we now discuss the generic propagation of ionization fronts through the protostellar disk (for the case of cataclysmic variables see Smak 1984 and Lin et al. 1985). It can be shown that outbursts which initiate near the inner edge of the disk and propagate outwards ("inside-out" outbursts) always have slow risetimes because the ionization front must proceed in a "snow plow" manner, moving up the surface density gradient in a direction contrary to the global flow of matter. In contrast, outbursts which are initiated near the outer edge of the unstable region and propagate inwards ("outside-in" outbursts) exhibit rapid risetimes because the ionization front proceeds down the surface density gradient and moves with the global flow of matter at "avalanche"

speed. The primary conclusion of this section is that with this thermal instability model, outbursts must initiate near $R_{\rm limit}$ and propagate inward to produce the rapid risetimes seen in FU Ori and V1057 Cyg.

It can be shown that an inward-propagating front travels faster than an outward-propagating front, and thus an outside-in outburst has a shorter risetime than an inside-out outburst. Because the propagation of a front requires sufficient mass transfer from the ionized region to bring the surface density of the neighboring annulus above the local critical value, the front propagates at a speed comparable to the rate of mass transfer across the ionization front, U_r. It can be shown from the equation of motion, $\Sigma U_r r = -3r^{1/2}(\partial \Sigma \nu r^{1/2}/\partial r)$, that the viscous flow of matter follows the relation

$$U_r = -3\frac{\nu}{r}\left(\frac{\partial \ln \Sigma}{\partial \ln r} + \frac{\partial \ln T_c}{\partial \ln r} + 2\right), \quad (3)$$

where ν is given in the α approximation by $\alpha c_s H$. When the term in parentheses is positive, the ionization front propagates inward; where it is negative, the ionization front propagates outward. Both sign and magnitude of the radial gradients of T_c and Σ therefore contribute to propagation of inward- and outward-moving fronts.

Radial gradients of T_c and Σ can be estimated from Figures 4*a* and 4*b*, respectively. This figure shows the onset of a typical triggered outburst and will be discussed more fully below. Initially both gradients are relatively flat: $\partial \ln T_c/\partial \ln r \sim 0$ and $\partial \ln \Sigma/\partial \ln r > -1$. As the triggered region begins to ionize and heat, the gradients become positive in sign on the inner edge of the ionized region and negative in sign on the outer edge. (The behavior of $\Sigma(r)$ between the two fronts is more complicated due to a local depletion caused by the spreading of this effectively isolated, high-viscosity annulus.) The magnitude of both gradients, however, is significantly larger on the inward edge of the ionized region than on the outward edge, and therefore the symmetry is broken. Current estimates agree with the Lin et al. (1985) derivation which suggests a typical gradient of $\sim r/H$ at the inner edge of the region undergoing ionization and ~ -1 at the outer edge. The inward-moving front therefore propagates at the rate $U_r \sim ac_s$ approximately r/H faster than the outward-moving front which travels at $\alpha c_s H/r$.

In both outside-in and inside-out outbursts, decline from the high state is governed by the slow radial propagation of the outward-moving front and so always occurs on a long timescale. Decay timescales may be modified due to effects not considered such as, for example, the self-illumination of the disk (i.e., the reprocessing of inner-disk photons in the outer disk). Self-illumination could have various dynamical effects such as prewarming the disk leading to an increased radial propagation of the outward-moving front, or it could stall the system in the outburst phase by prolonging the ionization of hydrogen in the transition region. Also the thermal structure of the disk during quiescence could be altered which might affect recurrence timescales (as in Bell, Lin, & Ruden 1991).

3.4. *Perturbation Parameters*

In this section a perturbation in surface density is introduced as a way of creating outbursts which initiate some distance from the central object. It may be that a mass transport mecha-

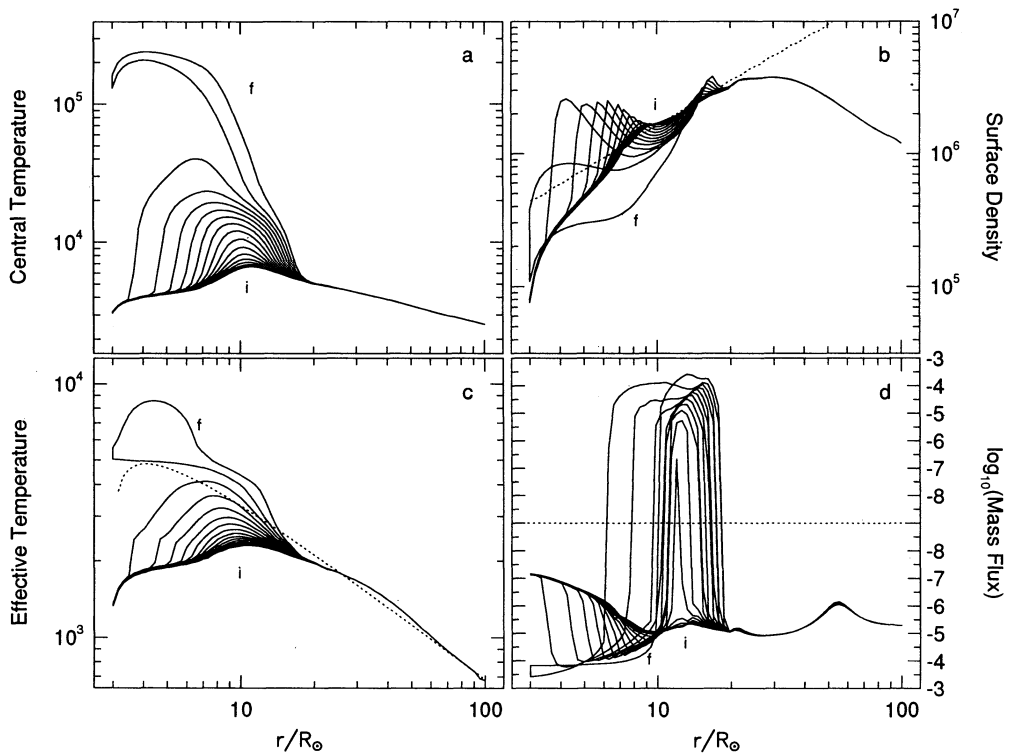

FIG. 4.—Onset of triggered model outburst. Radial disk evolution during time-dependent diffusion calculation for which $\dot{M}_{\rm in}$, M_p, $\Delta\Sigma/\Sigma$, and R_p equal 5×10^{-6} $M_\odot$ yr^{-1}, 0.02 $M_\odot$, 0.5, and 20 $R_\odot$, respectively. Successive snapshots (19) are separated by 1 yr intervals; initial and final epochs are marked i and f, respectively. Outburst begins near 10 $R_\odot$ initiating two ionization fronts marked by surface density maxima traveling away from ignition point. (*a*) $T_c(r)$. Midplane temperature (K). (*b*) $\Sigma(r)$. Surface density (g/cm^2). Dotted line marks critical surface density, $\Sigma_A(r)$. (*c*) $T_d(r)$. Surface temperature (K). Dotted line marks constant mass flux disk at $\dot{M}_{\rm in} = 5 \times 10^{-6}$ $M_\odot$ yr^{-1}. (*d*) $\dot{M}(r)$. Mass flux [$\log_{10}$ ($|M_\odot$ yr$^{-1}|$)]. Zero mass flux at dotted line: inflow below, outflow above.

nism more realistic than the ad hoc α-law viscosity used here (see, for example, the discussion in § 5.3) will spontaneously produce outside-in outbursts without requiring the invocation of an arbitrary perturbation.

In a series of trial cases a surface density perturbation is applied to the radial time-dependent evolution models during quiescence to evaluate the impact of such perturbations on the risetime and maximum disk temperature [$T_{max}(t)$] during outburst. Perturbations are added at the ambient temperature of the disk and are specified by three parameters: the total mass in the perturbation, M_p, the inner radius, R_p, and the fractional surface density excess, $\Delta\Sigma/\Sigma$. Given M_p and R_p, the outer edge of the perturbation, R_{po}, is determined by $\Delta\Sigma/\Sigma$ and M_p such that

$$M_p = \sum_{R_p}^{R_{po}} \left(\frac{\Delta\Sigma}{\Sigma}\right)\Sigma_0(r)A(r)\,, \qquad (4)$$

where $\Sigma_0(r)$ is the surface density at r before perturbation and $A(r)$ is the area of the annulus at r. The edges of the perturbation are crudely smoothed such that $\Delta\Sigma/\Sigma$ is reduced to one-third and two-thirds in the first and second perturbed zones and to whatever is required to bring the perturbation mass up to the specified M_p in the last perturbed zone.

Several mass-conserving trial runs are performed in which mass equal to M_p is removed from the disk either exterior to R_{po} or interior to R_p. Mass is subtracted in such a way that the minimum remaining surface density is no less than $0.1\Sigma_0$. As many zones are depleted as necessary to account for the mass in the perturbation. When the depleted region is exterior to the perturbed region, the duration of the outburst may be slightly shortened as the ionization front stalls when it enters the depleted region, but risetimes and spectral evolution are essentially unaffected. When the depleted region is interior to the perturbed region, however, the importance of the depleted region depends on the strength of the perturbation. If the perturbation is such that a local thermal runaway is triggered before significant viscous evolution has occurred (as when $\Delta\Sigma/\Sigma$ is large), then the depleted region has negligible effect on the course of the outburst. If, however, the perturbation is not sufficiently narrow or massive to trigger a *local* thermal runaway, then viscous processes merely fill up the depleted region and an outburst is prevented. Throughout the remainder of this work, the *non*-mass-conserving perturbation is used in which M_p is added to the disk without compensation.

The triggering of an outburst may proceed along a continuum between two extremes. A strongly localized perturbation results from a large value of $\Delta\Sigma/\Sigma$ and upon application immediately increases the value of the surface density above its local critical value $\Sigma_A(r)$, triggering a prompt outburst which initiates near R_p. Alternatively, the mass added by a perturbation may be so broad and shallow (small $\Delta\Sigma/\Sigma$) that the surface density is not directly increased above its local critical value. The mass left by the perturbation (M_p) will evolve viscously inward heating the disk as it goes ($Q^+ \propto \Sigma$). If M_p is large enough, the critical surface density may still be exceeded first far from the central object.

The effects of application of one such triggered outburst are demonstrated through the time-dependent evolution of $T_c(r)$, $\Sigma(r)$, $T_d(r)$, and $\dot{M}(r)$ at 1 yr intervals in Figures 4*a–d*, respectively. The model is the result of a broad perturbation applied to an $\dot{M}_{in} = 5 \times 10^{-6}\ M_\odot\ \mathrm{yr}^{-1}$ disk with perturbation parameters $M_p = 0.02\ M_\odot$, $\Delta\Sigma/\Sigma = 0.5$, and $R_p = 20\ R_\odot$. (Note the lessening of the inward mass flux at about 50 $R_\odot$ not seen in the self-regulated BL 94 models which carries away the excess angular momentum of the perturbation mass.) The added mass diffuses inward resulting in an increase of the surface density above $\Sigma_A(r)$ (dashed line in Fig. 4*b*) at about 10 $R_\odot$. The initiation of hydrogen ionization triggers both inward- and outward-propagating fronts from the ignition point. Because in a given system $\dot{M}(\Sigma_A)$ is a strongly increasing function of radius, initiation of instability at large radius results in an outburst with larger characteristic temperature and mass flux than an outburst initiated at small radius. Triggered (rapid risetime) outbursts thus tend to be hotter and to have higher outburst mass fluxes than self-regulated (slow risetime) outbursts in agreement with observations. Application of a perturbation can prematurely drain a supercritical disk such that the next (self-regulated) outburst may be significantly delayed.

3.5. *Effect of Perturbation on $M_B(t)$*

A triggered outburst differs from a self-regulated outburst principally in that the first initiates two fully developed ionization fronts while the latter initiates only one. The evolution of a triggered outburst light curve, $M_B(t)$, may thus be divided into two phases: (1) an initial sharply peaked stage which is governed by the rapidly inward-propagating ionization front followed by (2) a more rounded, plateau stage regulated by the slow movement of the outward-propagating ionization front. Self-regulated outbursts have no inward-propagating front and are therefore only subject to the second phase. Further, the *duration* of the plateau phase is determined by R_{limit} which therefore suggests the degree of supercriticality of the disk undergoing outburst. This duality explains why outbursts resulting from perturbed, subcritical disks (as in Clarke et al. 1990) are strongly peaked and have essentially no plateau phase while outbursts from self-regulated, supercritical disks (as in Bell & Lin 1994) have no initial spike and are all slowly evolving plateau phase. The *shape* of an outburst light curve, in particular the relative dominance of the two phases, can therefore suggest the relative importance of the perturbation (if any) as well as the degree of supercriticality (if any) of the underlying disk.

These general arguments based solely on light curve *shape* can be used to suggest underlying disk properties of our three program objects (Fig. 1). The FU Ori light curve has a rapid risetime plus an extended plateau phase which suggests an outburst from a (1) triggered, (2) supercritical disk. The rounded light curve shape of V1515 Cyg suggests a "spikeless" or principally self-regulated outburst. The strong initial peak of the V1057 Cyg light curve suggests a triggered outburst, and the nearly but not entirely plateauless decay phase suggests an underlying marginally supercritical disk. The variety of light curves may thus (leaving aside for the moment the source of the trigger) be simply categorized by shape.

We have investigated the effect on the resultant $M_B(t)$ of varying M_p, $\Delta\Sigma/\Sigma$, and R_p independently through calculation of over 150 models (Bell 1993). An example showing the effect of varying the three perturbation parameters is shown in Figure 5. The benchmark perturbation (given by the solid line in each panel) is applied immediately after a self-regulated outburst to a disk with $\dot{M}_{in} = 5 \times 10^{-6}\ M_\odot\ \mathrm{yr}^{-1}$; this is a strongly supercritical disk so outbursts all have long plateau phases. This system is the one shown in Figure 4 with parameters $M_p = 0.02\ M_\odot$, $\Delta\Sigma/\Sigma = 0.5$, and $R_p = 20\ R_\odot$. Varying M_p from 0.0 to 0.02 $M_\odot$ (Fig. 5*a*) shows that additional mass somewhat lengthens the duration of the outburst ($\approx$15% over this

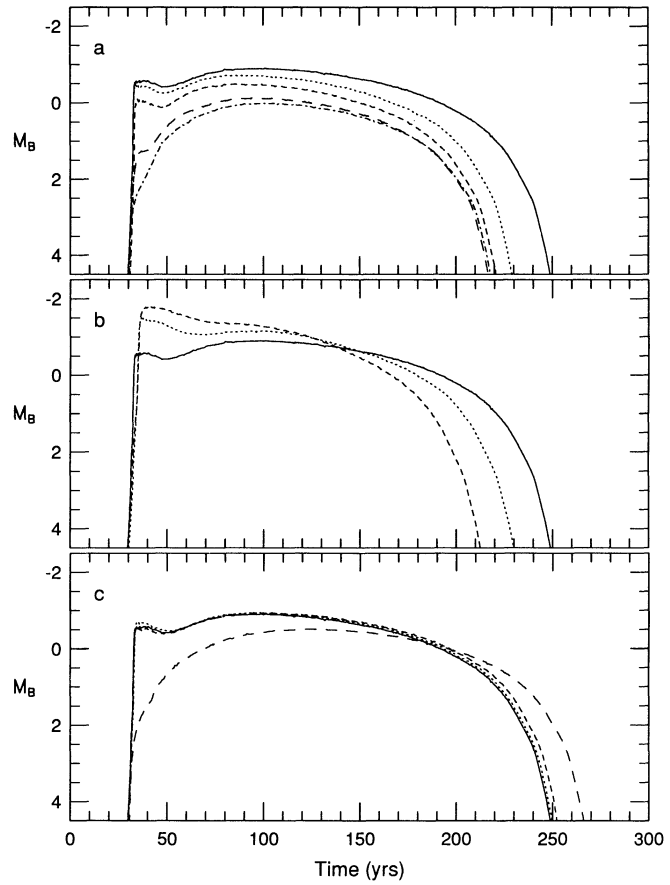

FIG. 5.—Parameter variations; dependence of $M_B(t)$ on M_p, $\Delta\Sigma/\Sigma$, and R_p. In all models $\dot{M}_{in} = 5 \times 10^{-6}\ M_\odot\ yr^{-1}$ ($R_{limit} \sim 25\ R_\odot$). The solid curve in each panel has benchmark perturbation M_p: 0.02 $M_\odot$, $\Delta\Sigma/\Sigma = 0.5$, and $R_p = 20\ R_\odot$. (*a*) $M_p = 0.02$, 0.01, 0.005, 0.001, and 0.0 $M_\odot$. (*b*) $\Delta\Sigma/\Sigma = 0.5$, 1.0, and 3.0. (*c*) $R_p = 8$, 13, 20, and 32 $R_\odot$.

range) as well as somewhat increasing the peak disk temperature, mass flux, and risetime, but the primary effect of increasing M_p is to increase the dominance of the initial spike phase of the outburst. The initially rapid rise (up to $M_B \sim 2$) of the spontaneous outburst ($M_p = 0$; dot-dash line) results from the fact that even the self-regulated outburst does not initiate at the very inner edge of the disk but at about two stellar radii and consequently also has a brief outside-in phase (BL 94). Note also that perturbed models have consistently higher peak magnitudes than the unperturbed model. As well as being more rounded in shape, self-regulated models tend to have peak values somewhat lower than comparable triggered models.

Larger fractional surface density excess, $\Delta\Sigma/\Sigma$, results in larger peak disk temperature and mass flux, quicker decay after outburst, and quicker onset of the outburst after application of the perturbation (Fig. 5*b*); larger $\Delta\Sigma/\Sigma$ also results in a somewhat longer risetime (the initial rise varies between 1 and 5 yr). Finally, variations in R_p are investigated in Figure 5*c*. For this relatively broad perturbation with R_p inside the unstable inner region ($R_{limit} \approx 25\ R_\odot$ for $\dot{M}_{in} = 5 \times 10^{-6}\ M_\odot\ yr^{-1}$) the exact value of R_p has *no impact* on the shape or magnitude of the outburst; if the inner edge of the perturbation falls beyond the unstable region, however, there is no rapid risetime, outside-in outburst but only a somewhat longer and slightly more intense slow risetime, inside-out outburst.

4. RESULTS

A successful theory of FU Ori outbursts must be able to reproduce the main features of observed light curves. The time-dependent code developed in BL 94 is used to compute theoretical light curves by assuming that the surface of the model disk radiates like a blackbody at the local effective temperature. The sloping of the disk is also neglected in these calculations, that is, relative areas only depend on the radial interval. Models whose M_B light curves match as closely as possible the observed outburst light curves for each of the three program Fuors are developed. The observed risetime of V1515 Cyg is matched with the self-regulated outbursts developed in BL 94. To reproduce the rapid risetimes of FU Ori and V1057 Cyg modest surface density perturbations are applied to supercritical disks during the quiescent state. As discussed above, the details of the perturbation are not as important as the fact that their application changes the outburst from one which is initiated near the star (i.e., "inside-out") to one which is initiated near the outer edge of the unstable region of the disk ("outside-in"). Throughout this work, *models are not corrected for either distance or extinction.* Data are compared to models using estimated corrections given in Table 1.

Actual fits to specific objects are derived in § 4.1 *solely on the basis of $M_B(t)$ light curves.* Resulting models are then compared to other observational aspects of Fuors to test the predictive power of simple light curve fitting. We examine in turn the evolution of photometry and colors in § 4.2 and line widths in § 4.3. In § 4.4 the generic evolution of model SEDs is discussed to isolate how different spectral regions can tell us about the evolution of the underlying ionization front. Finally the low-mass-flux phase of evolution is discussed (§ 4.5), and suggestions are made about how to identify Fuors in quiescence.

4.1. *Light Curve Fitting*

We now discuss specific fits to the three program objects. Model parameters are summarized in Table 2. Also given are "current" values (recorded at the end of light curve fitting) of maximum disk temperature (T_{max}), mass flux through the innermost zone ($\dot{M}_{acc}$), and the largest radius with fractional ionization greater than 10^{-6} (R_t).

Note that uncertainties in extinction allow almost a magnitude in leeway in fitting $M_B(t)$ (cf. Table 1). One value for the extinction is adopted. Note also that observations (especially at early times) show a great deal of scatter. For our given choice of correction there is *more than one model* which fits

TABLE 2

PARAMETERS AND RESULTS OF OUTBURST MODELS

Model	$\dot{M}_{in}$ ($M_\odot\ yr^{-1}$)	M_p ($10^{-2}\ M_\odot$)	$\Delta\Sigma/\Sigma$	R_p ($R_\odot$)	T_{max}[a] (K)	$M_* \dot{M}_{acc}$[a] ($M_\odot^2\ yr^{-1}$)	R_t[a] ($R_\odot$)
A1.....	3×10^{-6}	1.0	3	13	7800	5.5×10^{-5}	35
A2.....	3×10^{-6}	1.0	10	13	7800	5.8×10^{-5}	35
A3.....	5×10^{-6}	0.7	5	20	8000	6.5×10^{-5}	35
B1.....	1×10^{-6}	...	...	...	7900	6.0×10^{-5}	26
B2.....	8×10^{-6}	...	...	...	7700	5.3×10^{-5}	25
B3.....	5×10^{-6}	0.1	4	34	7900	6.1×10^{-5}	26
C1.....	1×10^{-6}	0.2	3	10	6700	2.6×10^{-5}	24
C2.....	1×10^{-6}	0.2	5	10	6700	2.6×10^{-5}	24
C3.....	8×10^{-7}	0.3	5	10	6900	3.0×10^{-5}	24

[a] "Current" values at end of light curve fitting.

each program light curve to a high degree of accuracy. Allowing for uncertainties in extinction, there are therefore many possible models which could fit any given Fuor light curve. More exact specification of model parameter ranges would be possible if extinctions were more precisely known. Also, because the central object masses are not known, an additional uncertainty is introduced into the model fits mass fluxes.

In Figure 6*a* are shown three outburst models which satisfactorily reproduce the general features of the 1936 outburst of FU Orionis (models A1, A2, and A3); data dereddened by the factor given in Table 1 are shown for comparison as small dots. All three result from triggered supercritical disks with differing perturbation parameters (Table 2). All three of the models reproduce not only the light curve shape but also the current absolute B magnitude (-0.5) of FU Ori. The current model maximum disk surface temperature, $T_{\max} \approx 7900$ K (Fig. 6*d*), modestly exceeds FU Ori's current temperature, 7200 ± 400 K (KHH 88), estimated from SED fitting under the constant-mass-flux disk assumption.

Figure 6*b* shows three outburst models which are patterned after the outburst of V1515 Cygnus (models B1, B2, and B3). Solid and dotted lines are self-regulated outbursts for which $\dot{M}_{\rm in} = 1 \times 10^{-5}$ and 8×10^{-6} $M_\odot$ yr^{-1}, respectively. The dashed line represents a modest perturbation (0.001 $M_\odot$) on a 5×10^{-6} $M_\odot$ yr^{-1} disk applied at large radius ($R_p > R_{\rm limit}$) which also matches the observations very well. Modeled disk temperatures ≈ 7900 K (Fig. 6*e*) somewhat exceed estimates of the current disk temperature of ≈ 7000 K (KHK 91). Because of the obscuring of the light curve by the 1980 dust condensation event, we do not attempt to fit the observations at late times.

Figure 6*c* shows three light curves which attempt to match observations of V1057 Cygnus (models C1, C2, and C3). None of the three (nearly coincident) models are entirely satisfactory because all fail to rise and fall as sharply as observed and fail to attain the luminosity seen near peak light. Nevertheless the "current" (measured at the end of light curve fitting) disk temperatures of 6800 K (Fig. 6*f*) fall within the range of the estimated peak disk temperatures of 6600 ± 400 K (Hartmann & Kenyon 1985). Note also that V1057 Cyg is estimated to be observed nearly pole-on (Table 1); short-wavelength boundary layer effects which are not considered in this work may be particularly important in this object especially during the earliest stages of outburst.

The light curves of FU Ori and V1515 Cyg are well fit by the models. The poor fit to the early light curve of V1057 Cyg may be improved with a small increase in the value of the high-state viscosity α-parameter. A larger value of α would result in more rapid viscous evolution during outburst and consequently shorter timescales. A factor of 10 larger results in unacceptably short recurrence and outburst timescales (BL 94). A factor of 2, however, might improve this fit without detrimentally impact-

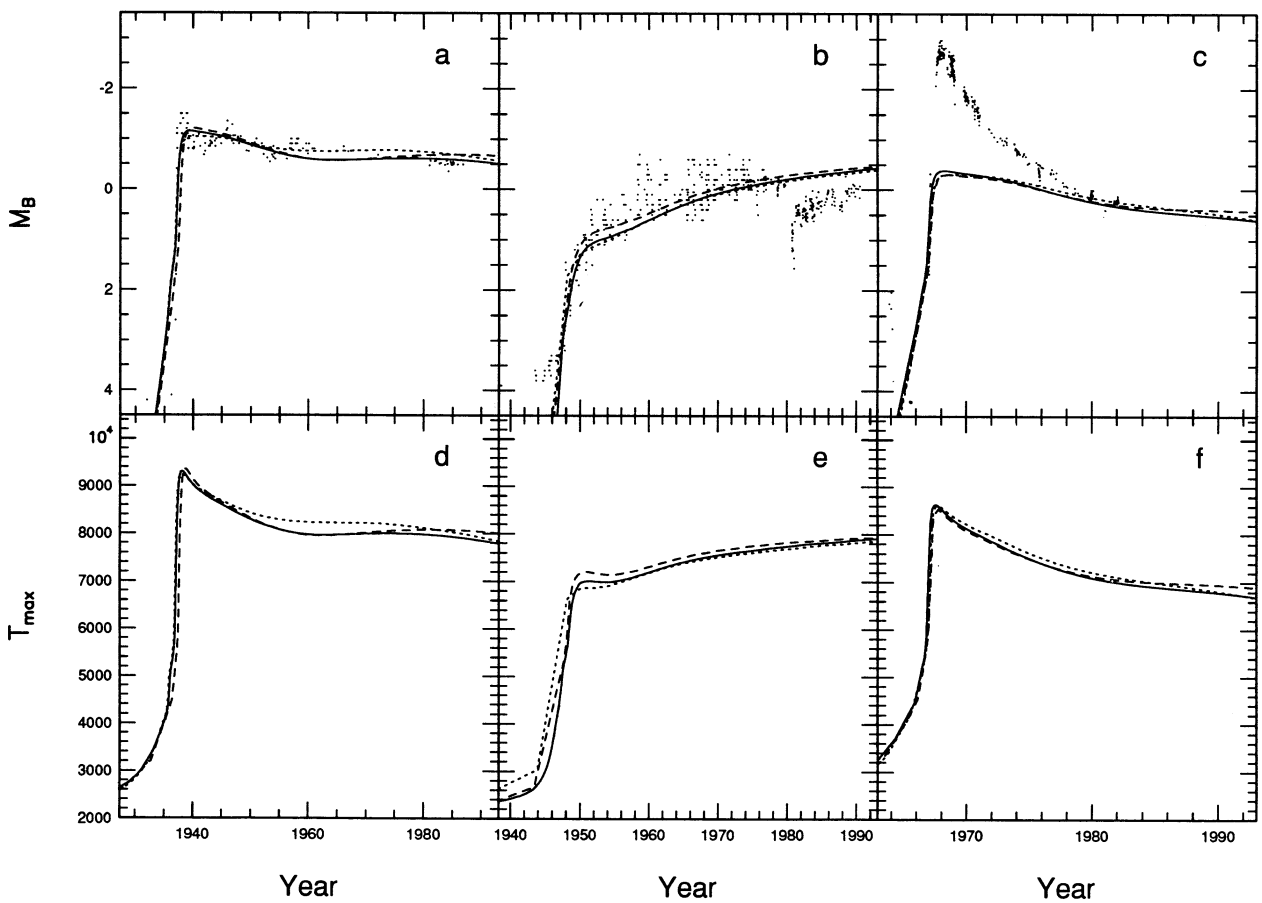

FIG. 6.—Model light curves; $M_B(t)$ and $T_{\max}(t)$. Dots represent observations. (*a*) FU Ori–like models. Solid, dotted, and dashed lines refer to cases A1, A2, and A3, respectively; model parameters are given in Table 2. (*b*) V1515 Cyg–like models. Solid, dotted, and dashed lines refer to cases B1, B2, and B3, respectively. (*c*) V1057 Cyg–like models. Solid, dotted, and dashed lines refer to cases B1, B2, and B3, respectively. (*d*), (*e*), and (*f*) Evolution of maximum disk temperatures for the A, B, and C models, respectively.

ing recurrence timescales. Although a larger value of α also tends to raise disk temperatures during outburst, the quicker timescales would allow lower values of $\dot{M}_{in}$ for each fit which would in turn result in lower temperatures. In this way, slightly different parameters may, with a slightly larger value of α, result in lower peak temperatures more in line with what is estimated from observations for all three objects. Despite the listed discrepancies, the agreement of models with the observations is excellent.

4.2. *Photometric Evolution*

So far models have been matched to program objects entirely on the basis of the fitting of B-band light curves with somewhat arbitrarily chosen extinctions. In this section models are compared with observations of evolution at other wavelengths and at $B-V$ and $R-I$ colors as a test of the predictive power of the models. Several standard accretion disk relations are introduced to assist the interpretation of model evolution in terms of changing disk properties.

The changing temperature of the disk is important in understanding the evolution of magnitudes, colors, and spectral energy distributions. The BL 94 models make use of the no-torque inner boundary condition, $\Sigma(0) = 0$, which results in a disk with a maximum rotation (Ω) at the characteristic radius of $R_{char} = 1.36R_*$ (BL 94). Because local dissipation is proportional to Ω^2: $Q^+ = (9/4)\Sigma\nu\Omega^2$, the disk surface temperature is a maximum at R_{char}. For a steady-state, optically thick accretion disk, the condition of vertical thermal balance ($Q^- = Q^+$) and the equation of motion (BL 94, eq. [1]) can be combined to define the local disk surface temperature $T_d(r)$ as a function of the local mass flux $\dot{M}(r)$:

$$2\sigma T_d^4(r) = \frac{9}{4}\frac{\dot{M}(r)}{3\pi}\left(1-\sqrt{\frac{R_*}{r}}\right)\frac{GM_*}{r^3}. \quad (5)$$

This function, evaluated at $\dot{M} = 5 \times 10^{-6}\ M_\odot\ \mathrm{yr}^{-1}$, is represented by the dashed line in Figure 4*c*. The maximum disk surface temperature occurs at R_{char} and is given by

$$T_{max} = 5750\ \mathrm{K}\left[\left(\frac{M_*}{M_\odot}\right)\left(\frac{\dot{M}}{10^{-5}\ M_\odot\ \mathrm{yr}^{-1}}\right)\left(\frac{R_*}{3R_\odot}\right)^{-3}\right]^{1/4}. \quad (6)$$

Again, the effects of the reradiation of central object photons by either outer disk or infalling envelope are not included. It is clear from equations (5) and (6) that optical emission will only be produced by the disk when it has a high accretion rate, and then it is only produced by the hottest, innermost regions. Longer-wavelength data is relevant to larger disk radii.

The evolution of the broad-band photometry points B, K, and N (4400 Å, 2.2 μm, and 10.4 μm respectively) for the nine model outbursts are shown in Figures 7*a*, 7*b*, and 7*c*. Note that although all B-band light curves in each panel are nearly indistinguishable at early times, different models show some variety in decay times. Because the decay from the plateau phase is always controlled by the slowly moving, outward-propagating front, models show similar, relatively slow declines regardless of the risetime. Because the outer steady mass flux region provides unchanging long-wavelength radiation while mass flux through the inner disk provides constantly changing short-wavelength radiation, magnitudes change most at short wavelengths in agreement with observations of V1057 Cyg (KHH 88). Because the ionization front continues to propagate outward even after the inner mass flux has started to drop, radiation shifts to longer wavelengths, and objects continue to brighten at K long after they have begun to fade significantly at shorter wavelengths.

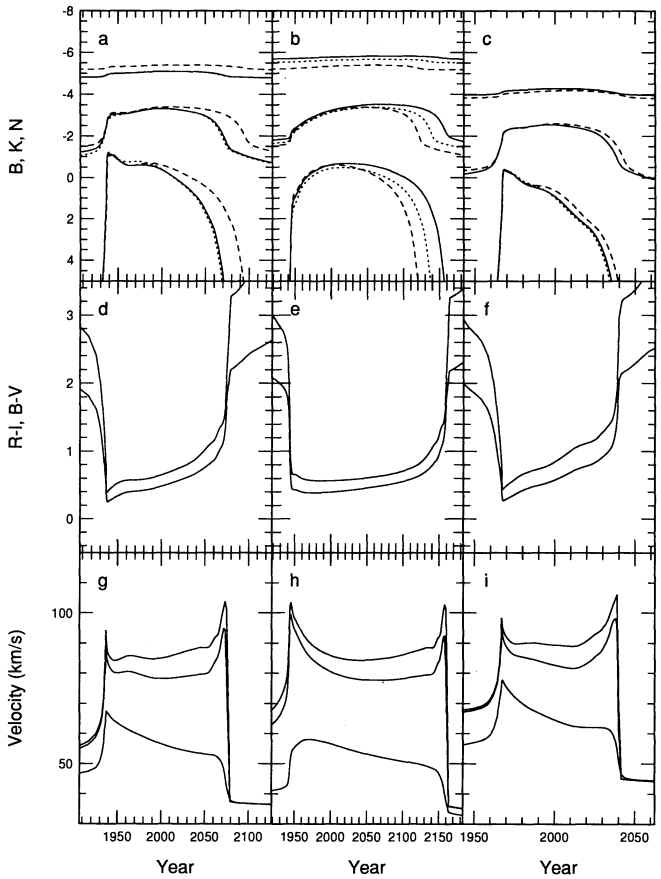

FIG. 7.—Evolution of model magnitudes, colors, and line-width velocities. (*a*), (*b*), and (*c*) B, K, and N magnitude evolution. (*d*), (*e*), and (*f*) $R-I$ and $B-V$ color evolution. (*g*), (*h*), and (*i*) Line-width velocity evolution at 4000 Å, 6000 Å, and 2.3 μm in km s^{-1}. (*a*), (*d*), and (*g*) FU Ori–like models. Solid lines represent A1; dotted and dashed lines (shown only for photometric evolution) represent models A2 and A3, respectively. Other quantities scale as $B(t)$. (*b*), (*e*), and (*h*) V1515 Cyg–like models. Solid, dotted, and dashed lines represent B1, B2, and B3, respectively. (*c*), (*f*), and (*i*) V1057 Cyg–like models. Solid, dotted, and dashed lines represent C1, C2, and C3, respectively.

Figure 7*d*, 7*e*, and 7*f* show the time evolution of the $B-V$ and $R-I$ colors for the A1, B1, and C1 models, respectively. For clarity, full evolution is not shown for the remaining six models. Colors of other models scale with time similarly to the B band. Changes in magnitude and color are again greatest at short wavelengths. Short-wavelength colors are greater than long-wavelength colors in agreement with observations, and the values of these colors are close to the colors measured for V1057 Cyg both before and during outburst (Fig.2).

4.3. *Line-Width Velocity Evolution*

In this section it is discussed that the outward movement of the ionization front during outburst naturally leads to a decreasing Keplerian line-width velocity. Near the end of the outburst, however, as the dropping mass flux in the inner annuli begins to dominate the evolution, line widths at wavelengths less than 1.5 μm are expected to increase.

Many radii contribute to the apparent line width at any given wavelength. The primary contributing radius: $R_v(\lambda)$, is roughly that radius specified by the Wien Law for which $T_d(\mathrm{K}) = 0.29/\lambda(\mathrm{cm})$. Although temperatures and therefore

fluxes are generally smaller for the outer annuli, the increasing areas are such that fluxes are often dominated by annuli at a radius somewhat larger than suggested by the simple Wien Law. A standard blackbody flux is calculated for each annulus:

$$B_\lambda[T_d(r)] = \frac{2hc^2}{\lambda^5}\left\{\exp\left[\frac{hc}{\lambda k T_d(r)}\right] - 1\right\}^{-1}, \quad (7)$$

where h, c, and k have their usual meanings. Velocities are flux weighted by the factor $W(r) \equiv B_\lambda[T_d(r)] \times A(r)$, where $A(r)$ is the area of the annulus at r. Again, the shape of the disk's surface is neglected and areas are given simply by $\pi(R_{i+1}^2 - R_i^2)$. The velocity for the wavelength λ is given by

$$V_\phi(\lambda) = \frac{\Sigma_{R_*}^{R_d} W(r)\sqrt{GM_*/r}}{\Sigma_{R_*}^{R_d} W(r)}, \quad (8)$$

where $R_* = 3\ R_\odot$ and $R_d = 20$ AU are the inner and outer disk radii, respectively. The effects of stellar radiation are not included. During outburst, this stellar contribution will be negligible. During quiescence, reprocessing of stellar light will cause velocities to deviate from what is suggested by this simple analysis.

Figures 7*g*, 7*h*, and 7*i* show the evolution of the Keplerian velocities at 4000 Å, 6000 Å, and 2.3 μm (shorter wavelengths display larger velocities) which correspond to disk temperatures of roughly 7200, 4800, and 1300 K, respectively. The sudden increase in velocity during the onset of outburst is due to the rapid increase in $T_{\max}$ which increases the flux from inner annuli "dragging in" the radius $R_v(\lambda)$. The decreasing line widths after peak light are due to increasing flux from larger radii as the ionization front propagates outward. As more of the disk enters the high state, rotational velocities are dominated by successively larger radii and therefore decrease. Near the end of outburst when the increasingly rapid drop in inner mass flux begins to dominate over the effect of the outward-propagating front, the conventional picture becomes appropriate. Uniformly dropping disk temperatures cause R_v to move in, and the line widths again increase.

Velocity reversal does not occur in the 2.3 μm line because disk annuli with the low temperatures it probes (1300 K) never reach the fully ionized state. For all wavelengths greater than about 1.5 μm (corresponding to a surface temperature of 2000 K) velocities are determined by the constant mass flux outer-disk annuli which never go into outburst. The dominant radius is only dragged in at all during outburst because the blackbody tails of the luminous inner annuli provide a bright, high-velocity component to the flux. It can be seen that R_v is never less than R_t at 2.3 μm. For example, the maximum line-width velocity of model C1 of ~ 80 km s^{-1} indicates that $R_v \sim 30\ R_\odot$, while Table 2 indicates that $R_t \sim 24\ R_\odot$. After peak light, as the inner disk fades, $R_v(\lambda)$ increases, and the velocity drops. This line-width velocity evolution is a strong prediction of the thermal accretion outburst model, and one which may be observationally testable.

4.4. *Spectral Energy Distributions*

In this section the generic evolution of model spectral energy distributions (SEDs) is examined. We do not attempt to specifically model particular sources, but discuss instead how the general slopes and evolution of model SEDs differ from the constant mass flux (CMF) models particularly in the 1–8 μm range. Shortward of 1 μm, the SED is expected to be strongly affected by the poorly understood inner boundary condition. Longward of 8 μm, radiation from the disk is overwhelmed by reprocessing in the geometrically thick infalling envelope. In particular discussion focuses on the *differences* between constant mass flux disks and disks for which mass flux varies with radius. As discussed above, the effects of the reprocessing of stellar and inner disk photons in the disk are not included.

Figure 4*c* shows several snapshots of the surface temperature distribution for a model system making the transition from quiescence to outburst. The dotted line in this figure represents the radial distribution of surface temperature for a disk with mass flux equal to the input value of $\dot{M}_{\rm in} = 5 \times 10^{-6}\ M_\odot$ yr^{-1}. In the outer disk ($r \gtrsim 25\ R_\odot$), the disk has the temperature distribution of a steady disk at the input mass flux rate. In the inner disk, however, mass flux and temperature distribution differ considerably from what is expected from a constant mass flux system. During quiescence the inner-disk mass flux is smaller than $\dot{M}_{\rm in}$ so the disk temperatures are lower than in a CMF disk accreting at $\dot{M}_{\rm in}$; during outburst, mass fluxes and therefore temperatures are correspondingly larger. In this section the effect of this break in mass flux on resulting spectral energy distributions is investigated.

Spectral energy distributions are calculated by summing the standard blackbody relation (eq. [7]) over all radii. Spectra are normalized to a distance of 10 pc. Although the dominant contribution to the disk's SED comes from the active inner annuli, to avoid the long-wavelength distortions which can result from a smaller radius cutoff (Bell 1993), $T_d(r)$ is calculated from $R_* = 3\ R_\odot$ to the outer edge of the model disk at 0.5 AU from time-dependent results and out to $R_d = 20$ AU from equation (5) for a constant mass flux disk accreting at $\dot{M}_{\rm in}$.

Figure 8 shows time-dependent SEDs of disk model B1 (a self-regulated model with $\dot{M}_{\rm in} = 1 \times 10^{-5}\ M_\odot$ yr^{-1} during the rise to peak light (*a*) and during the decay after peak light (*b*). These figures illustrate how the propagation of the underlying ionization front affects the spectral evolution. Throughout the evolution, the region beyond 8 μm remains essentially constant. This part of the SED is produced by the outer disk which is relatively unaffected by the outburst in the inner disk. It can be seen that the constancy at 4.8 μm noted in V1057 Cyg (KHH 88) is a natural consequence of the thermal outburst model. Qualitatively similar to the behavior seen in V1057 Cyg, decay after peak light occurs first at short then at longer wavelengths. With the inclusion of reprocessing of light from the inner disk and central object by the infalling envelope (as in KH 91), the radiation beyond 8 μm is expected to rise and fall with the short-wavelength radiation (KH 91) as in Figure 3.

The details of these model SEDs can be understood as tracing the movement and evolution of the outward-moving thermal front through the protostellar disk. To assist the discussion, a series of arbitrary or "toy" models are developed in which equation (5) is used to create an artificial disk where inner and outer mass fluxes and the transition radius ($\equiv R_j$) may be varied independently. Note that this procedure assumes that local energy generation is strictly equal to local radiative losses (i.e., vertical thermal balance is assumed). The effects are discussed of (1) differing inner and outer mass fluxes, (2) the radius at which such transition occurs, and (3) deviation from vertical thermal balance. Note that this analysis assumes that the object may be perfectly dereddened and is observed face-on although in practice the extinction to any object and its inclination are parameters in the fitting procedure (e.g., KHH 88).

Figure 9*a* shows the effect on the resulting SED of varying the inner mass flux, (3, 10, and 30) $\times 10^{-6}\ M_\odot$ yr^{-1}, while

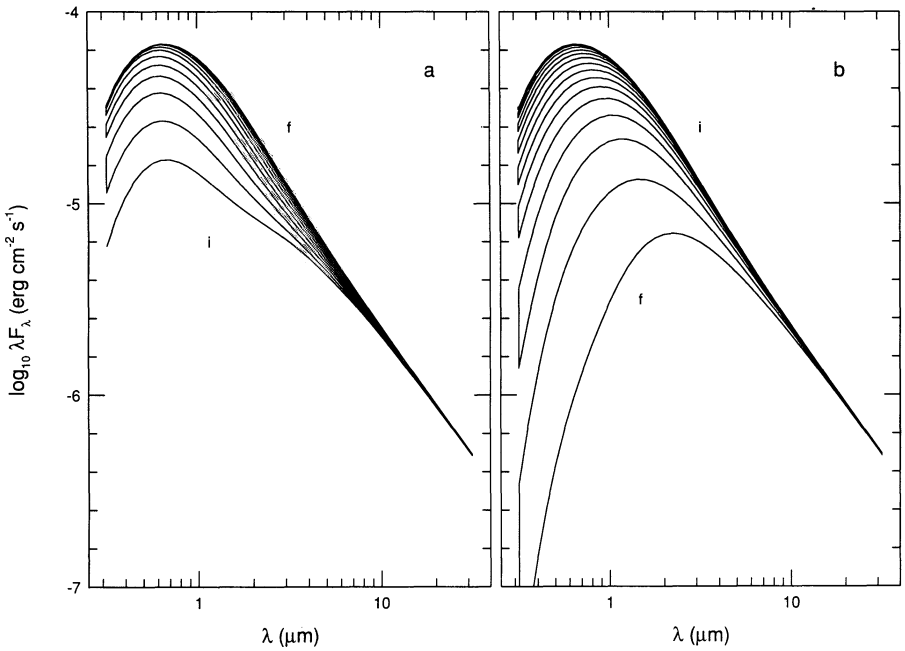

FIG. 8.—Time evolution of self-regulated Model B1 spectral energy distribution before (*a*) and after (*b*) peak light at 10 yr intervals. Note near constancy beyond 8 μm and decrease in infrared slope during post–peak light evolution.

holding constant the outer mass flux, $10^{-6}\ M_\odot\ \mathrm{yr}^{-1}$, and transition radius, $R_j = 30\ R_\odot$. Dotted lines indicate SEDs of constant mass flux (CMF) disks. Models are reasonably well fitted by the CMF approximation out to a few microns. Beyond this wavelength, SEDs have significantly steeper slopes than CMF disks. The effect of differing inner and outer mass fluxes may be detectable in some Fuors in that dereddened SEDs dip from best-fit CMF models in the 2–8 μm region for V1057 Cyg, FU Ori (KHH 88, Figs. 2*a*, 2*b*), and V1515 Cyg (KHK 91, Fig. 5). This effect is masked at longer wavelengths by the large, long-wavelength excesses commonly associated with FU Orionis variables which are thought to be caused by reprocessing in circumstellar envelopes. Nevertheless it is clear that if the decline from peak light is the result of a decline in mass flux in the inner disk while the outer disk continues to transport matter at a constant rate, the slope of the SED in the 1–8 μm

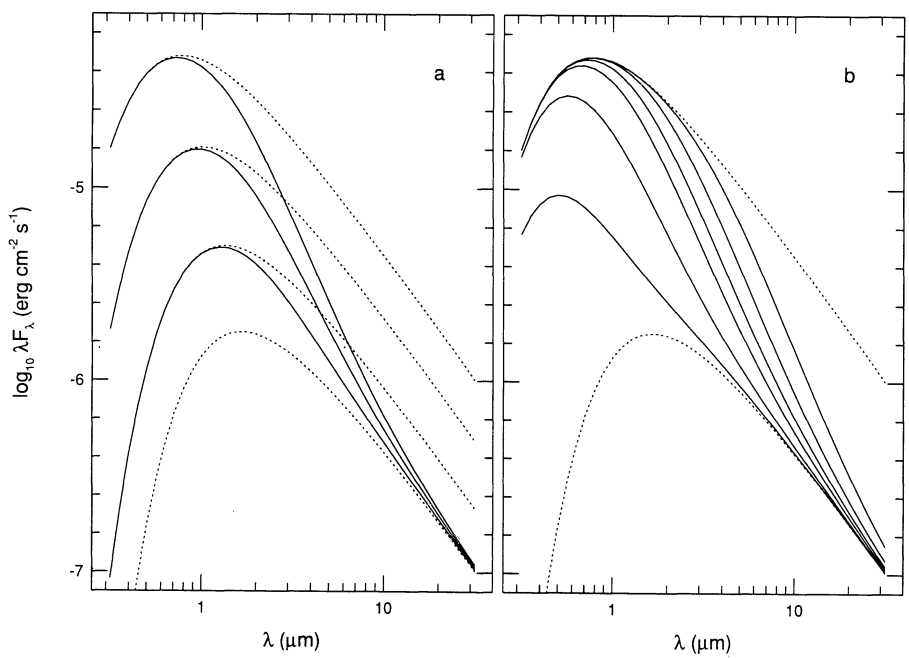

FIG. 9.—SEDs of arbitrary models. (*a*) Variation of inner mass flux. Joining radius $R_j = 30\ R_\odot$. Solid lines represent disks with inner and outer mass fluxes of (3, 10, and 30) $\times\ 10^{-6}$ and $1 \times 10^{-6}\ M_\odot\ \mathrm{yr}^{-1}$, respectively. Dotted lines are constant mass flux disks at (1, 3, 10, and 30) $\times\ 10^{-6}\ M_\odot\ \mathrm{yr}^{-1}$. (*b*) Variation of joining radius. Solid lines have inner and outer mass fluxes 3×10^{-5} and $1 \times 10^{-6}\ M_\odot\ \mathrm{yr}^{-1}$, respectively, and transition radii R_j of 5, 10, 20, 30, 50, and 100 $R_\odot$. Dotted lines are constant mass flux disks at $\dot{M}$ = (1 and 30) $\times\ 10^{-6}\ M_\odot\ \mathrm{yr}^{-1}$. Note decrease in peak wavelength for small R_j.

region is expected to decrease over time. This effect is seen in modeled disks (Fig. 8*b*) and is similar to the effect seen in the SED evolution of V1057 Cyg (Fig. 3).

Figure 9*b* demonstrates the effect of holding constant inner and outer mass fluxes: 3×10^{-5} and 1×10^{-6} $M_\odot$ yr^{-1}, respectively, while varying the joining radius: $R_j = 5$, 10, 20, 30, 50, and 100 $R_\odot$. Only a small high-mass flux inner region is necessary to dominate the spectrum at short wavelengths; for R_j as small as 20 $R_\odot$ (1/10 AU) the peak of the SED is dominated by the inner high mass flux region. For R_j smaller than 20 $R_\odot$, however, *the inner high mass flux region systematically decreases the peak wavelength of the SED.* All models in Figure 9*b* have the same maximum surface temperature and mass flux, but those with $R_j \lesssim 20$ $R_\odot$ have SEDs which peak at significantly shorter wavelengths. This effect may have important consequences for the interpretation of Fuor SEDs.

Increasing the transition radius beyond 20 $R_\odot$ has the effect of increasing emission beyond 1 μm bringing successively longer wavelengths into closer agreement with the constant mass flux model. The observational detection of changes in the transition radius would provide a direct measure of the high-state α viscosity parameter because the propagation of such fronts depends on the value of α (§ 3.3).

Figure 10*a* compares the "current epoch" of model B1 (solid line) with the dereddened data for V1515 Cyg (points; KHK 91). Unlike the photometry points and colors above, dereddening here is taken directly from KHK 91 from the best-fit modeling of the SED as a CMF disk. The time-dependent SED is fitted to the data at the 1.65 μm point; the shift is less than 0.1 in $\log_{10}$ (λF_λ). Model results show that the mass flowing through the inner annulus at this epoch is $\dot{M}_{\rm acc} = 6 \times 10^{-5}$ $M_\odot$ yr^{-1} (Table 2). Also shown in this figure are two CMF disks with mass fluxes equal to $\dot{M}_{\rm acc}$ (dotted line; fit at 1.65 μm by shifting vertically by 0.4) and 4×10^{-5} $M_\odot$ yr^{-1} (dashed line; shifted by 0.3). Note the identical infrared slopes of the two CMF models. In the 2–8 μm region, the slope is best fitted by the time-dependent model. Shortward of 2 μm, the fit could be improved by (1) the use of atmospheric models instead of the simple blackbody models used and (2) an adjustment in the extinction.

To conclude our qualitative discussion of how time-dependent SEDs differ from CMF SEDs, we now consider in some detail the current epoch SED of model B1 which is shown by the solid line in Figure 10*b*. The dotted line corresponds to a constant mass flux model at $\dot{M}_{\rm acc} = 6 \times 10^{-5}$ $M_\odot$ yr^{-1}. Because the time-dependent SED peaks at a *shorter* wavelength than the $\dot{M}_{\rm acc}$ model, both $T_{\rm max}$ and $\dot{M}_{\rm acc}$ might be *overestimated* from the observations if SED fitting assumed a CMF disk. Model results show further that $\dot{M}_{\rm in} = 1 \times 10^{-5}$ $M_\odot$ yr^{-1} for this model, and for the epoch currently under discussion the ionization front is about 26 $R_\odot$. As Figure 9*b* indicates, the spectroscopic impact due to differing inner and outer mass fluxes depends critically on the joining radius R_j. The dashed line in Figure 10*b* results from a toy disk model with inner and outer mass fluxes 6×10^{-5} and 1×10^{-5} $M_\odot$ yr^{-1}, respectively, and $R_j = 26$ $R_\odot$. This improves the fit dramatically at longer wavelengths but still produces a surprisingly poor fit at short wavelengths.

A clue to the nature of the remaining discrepancy is gained from the observation that the model has a $T_{\rm max}$ of 7900 K (Fig. 6*b*) which is *less* than the CMF model for a mass flux of 6×10^{-5} $M_\odot$ yr^{-1} of 9000 K (eq. [6]). The time-dependent model therefore has a lower surface temperature than implied by its mass accretion rate which is to say that the model deviates from vertical thermal balance in the sense that its energy content is greater than implied by its surface flux, that is, the

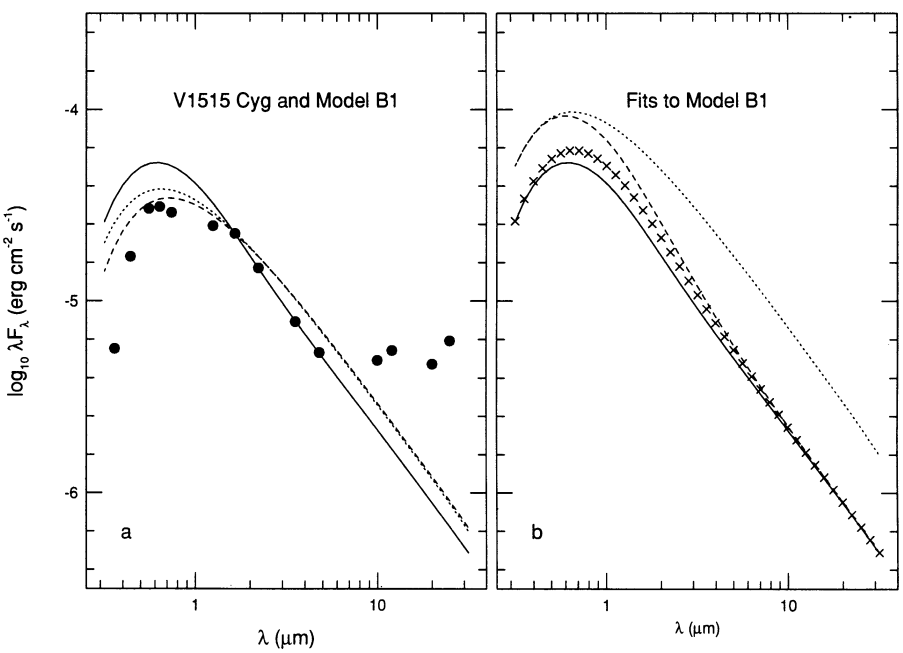

FIG. 10.—Observational and constant mass flux fits to model B1. (*a*) Dereddened SED data (points; KHK 91), two constant mass flux (CMF) disks with mass fluxes equal to (6 and 4) $\times 10^{-5}$ $M_\odot$ yr^{-1} (*dotted and dashed lines*, respectively), and "current epoch" of model B1 (*solid line*). Models are matched to data at 1.65 μm. Note infrared slope better fitted by time-dependent model than by CMF assumption. (*b*) Detailed toy model fits to current epoch of model B1 (*solid line*). CMF disk with mass flux of $\dot{M}_{\rm acc} = 6 \times 10^{-5}$ $M_\odot$ yr^{-1} (*dotted line*). Split disk toy model with inner mass flux of $\dot{M}_{\rm acc}$, outer mass flux of 1×10^{-5} $M_\odot$ yr^{-1}, and transition radius of 26 $R_\odot$ (*dashed line*). Toy model which accounts for deviation from vertical thermal balance (*crosses*) with same outer mass flux and joining radius but with inner mass flux of 4×10^{-5} $M_\odot$ yr^{-1} provides best fit to time-dependent SED.

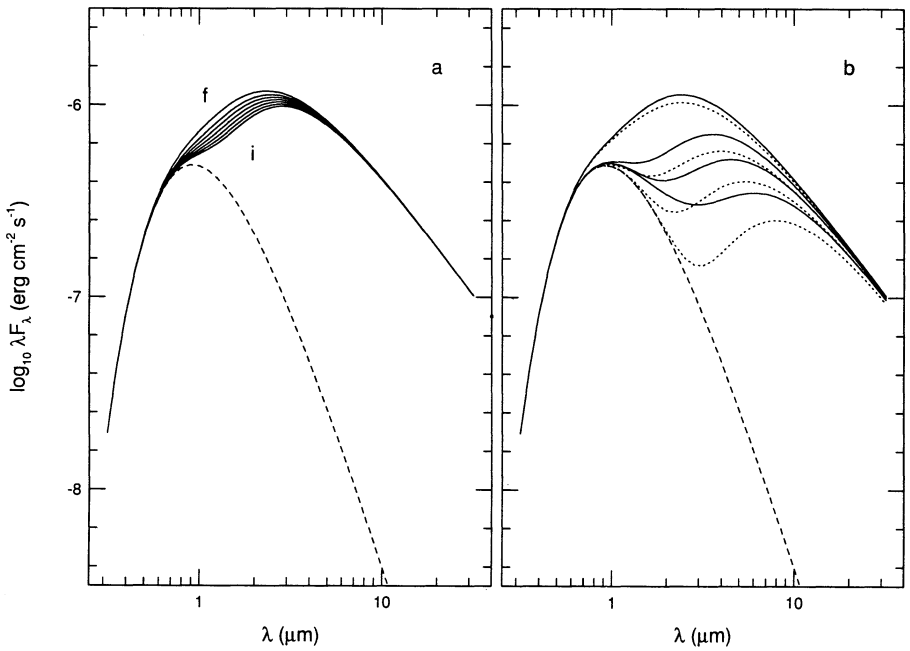

FIG. 11.—SEDs during quiescence including stellar contribution for which $R_* = 3\ R_\odot$, $T_* = 4000$ K (*dashed line*). (*a*) Time-dependent model results (7 epochs) at 50 yr intervals for $\dot{M}_{in} = 10^{-6}\ M_\odot\ yr^{-1}$ disk between outbursts. (*b*) Toy calculations. *Solid lines*: Inner and outer mass fluxes 10^{-7} and $10^{-6}\ M_\odot\ yr^{-1}$, respectively. Transition radii R_j 10, 20, 30, and 50 $R_\odot$. *Short dashed lines*: same but with inner mass flux 0 $M_\odot\ yr^{-1}$.

disk is storing energy. The effective temperature implied by a given mass flux under the vertical thermal balance approximation, T_{VTB}, is related to the actual surface temperature, T, at a given radius by the fractional heat imbalance, $\mathscr{F}$, through the relation

$$\mathscr{F} = \frac{Q^- - Q^+}{Q^- + Q^+} \approx \frac{T^4 - T_{VTB}^4}{T^4 + T_{VTB}^4} \Rightarrow T^4 = \frac{(1+\mathscr{F})}{(1-\mathscr{F})}\, T_{VTB}^4 . \quad (9)$$

In the BL 94 models, a typical deviation from VTB during outburst is $\mathscr{F} \approx -20\%$. While this fractional heat imbalance results in only a 10% difference in the surface temperature, $T \approx 0.9 T_{VTB}$, because $\dot{M} \sim T^4$, there is a 30% difference in the estimated mass flux; $\dot{M} \approx 0.7 \dot{M}_{VTB}$. If T_{max} is observed from high-resolution spectra and used to estimate $\dot{M}$, mass fluxes will therefore tend to be underestimated.

The SED given by crosses in Figure 10*a* represents application of the $\mathscr{F} = 20\%$ approximation which reproduces quite well the output from model B1 at the current epoch. Assuming that the departure from VTB is taken to be -20%, three parameters must be specified to fit the SED: inner and outer mass fluxes = 10×10^{-5} and $10^{-5}\ M_\odot\ yr^{-1}$, respectively, and $R_j = 26\ R_\odot$.

4.5. *The Quiescent Phase*

The thermal outburst model put forth in this paper suggests that for every system in outburst, 3–10 should be in quiescence. If so, where are all these systems? In this section, it is discussed that most of the systems subject to FU Orionis–type outbursts are likely to be embedded YSOs of ages up to about 10^5 yr. Spectral energy distributions of quiescent models are presented (§ 4.5.1), and recent work (Kenyon et al. 1993a; Lin et al. 1994) is discussed (§ 4.5.2) suggesting statistical evidence for the existence of quiescent Fuors.

4.5.1. *Quiescent Fuor SEDs*

The FU Orionis outburst model presented in this work requires a steady infall in the outer region of the disk of a few times $\times 10^{-6}\ M_\odot\ yr^{-1}$. Dusty envelopes with these large infall rates are thought to exist around not only many of the identified FU Orionis variables (KH 91) but also around all of the 21 embedded stars observed in a recent survey of the Taurus-Auriga molecular cloud (Kenyon et al. 1993a). Infall rates of this magnitude are associated with objects that have flat and rising spectra (Adams et al. 1987). Unfortunately, there is little or no early infrared photometry of an FU Orionis system which would indicate the presence or absence of an IR excess prior to outburst.

During quiescence, accretion from the outer disk accumulates near R_{limit} because the mass flux interior to this point is much smaller than the infall rate. The spectrum from such an object will look like a constant mass flux disk accreting at the infall rate, but with an inner edge of R_{limit}. Because the temperature of this inner edge is always ~ 2000 K (BL 94), resultant SEDs are expected to peak at a few microns. Figure 11*a* shows a series of SEDs from a time-dependent model disk with $\dot{M}_{in} = 10^{-6}\ M_\odot\ yr^{-1}$ between outbursts. A 3 $R_\odot$ central object with T_* of 4000 K (dashed line) has been added to the disk SED.[4] The time-dependent disk model (solid lines) is shown at 50 yr intervals. The SED shifts to shorter wavelengths as the disk heats up prior to its next outburst. Very few optically visible T Tauri stars have the substantial IR excess suggested by these model results, but embedded objects with flat or rising spectra may disguise this feature with long-wavelength radiation from reprocessing by outer disk or circumstellar envelope.

[4] Again we do not include the effects of a passive, reprocessing disk.

Figure 11*b* shows toy models of quiescent-Fuor disks which suggest that the inner low-mass flux region may be interpreted as a gap. Solid lines are models with inner and outer mass fluxes 10^{-7} and 10^{-6} $M_\odot$ yr^{-1}, respectively, with $R_j = 10$, 20, 30, and 50 $R_\odot$. Models represented by dotted lines have the same outer mass flux and transition radii but empty inner disks (i.e., the mass flux of the toy model is set to zero). This effect may be important in explaining the SEDs of the more massive YSOs known as Herbig Ae/Be stars (Hillenbrand et al. 1992; Bell 1994).

A strong test of a quiescent Fuor candidate would be the identification of the 2.3 and 4.6 μm CO absorption features generally seen in FU Orionis variables. When present in T Tauri objects, CO features are generally in emission (Carr 1988). In Fuors, CO absorption is thought to occur because of the strong vertical temperature gradients which arise when internally generated energy (as from viscous dissipation) is stronger than external heating (as from the star or inner disk). When the disk is passively reradiating light from the central object (as in the T Tauri case), radiation comes from a hot chromosphere on the disk's surface, so features, when present, are in emission. Figure 11 suggests that in quiescent Fuors, the luminosity between 2 and 5 μm will be dominated by disk emission. Even in sources with flat and rising spectra the contribution due to reprocessing may still be small at this wavelength. Features arising from the disk could be distinguished from CO absorption in the infalling envelope or in the star as disk features should be broadened by the rapid Keplerian rotation of the disk. Identification of broad CO absorption features would greatly strengthen the identification of a quiescent Fuor.

4.5.2. *Candidate Quiescent Fuors*

The Kenyon et al. (1993a) survey of 21 embedded protostars in the Taurus-Auriga molecular cloud found that all objects had luminosities which were considerably smaller than expected from estimated accretion rates under the assumption that such accretion proceeds directly down to the star. Further, luminosities of embedded "Class I" objects are observed to be systematically smaller ~ 1 $L_\odot$ than expected from theoretically (Shu, Adams, & Lizano 1987) and observationally (Kenyon et al. 1993a) derived mass fluxes ~ 30 $L_\odot$ (Kenyon et al. 1994). Observations of ultraviolet spectra (Valenti, Basri, & Johns 1993) confirm that matter is not accreting onto the central star at the rates expected for infalling envelopes. (See also Blondel et al. 1993 in the context of the more massive Herbig Ae/Be stars.) All of these things suggest that accretion through an envelope does not necessarily imply accretion directly onto the central star. This "luminosity problem" finds natural explanation in the context of the models currently under discussion in which accreting mass is halted some distance from the central object and accumulates in the disk.

Recent work by Lin et al. (1994) suggests a particular object, HL Tau, as a candidate for an FU Orionis object in quiescence. HL Tau is a source whose spectrum is flat out to 100 μm. HL Tau is known to be a continuum source (there are no optical absorption lines from which to assign spectral type) as was V1057 Cyg before outburst. HL Tau is also associated with a jet and has a magnitude similar to the $M_B \approx 4$ seen in all Fuors before outburst.

The strongest evidence pointing to HL Tau as a quiescent Fuor comes from recent millimeter maps by Hayashi, Ohashi, & Miyama (1993) which suggest a large infall mass flux of $(5 \pm 2) \times 10^{-6}$ $M_\odot$ yr^{-1} through the envelope at a distance of some 700 AU from the central object. This agrees with a recent SED analysis which suggests an infall rate for HL Tau of about 4×10^{-6} $M_\odot$ yr^{-1} (Calvet et al. 1994). In contrast to this, an upper limit to the rate of mass accretion onto the central star can be derived by taking $L_{\rm acc} = 0.5GM_*\dot{M}_*/r$ for a 3 $R_\odot$ central object from the extinction-corrected bolometric stellar luminosity of $L_* = 0.9$ $L_\odot$ (Beckwith et al. 1990) of 2×10^{-7} $M_\odot$ yr^{-1}. There is an additional clue to unsteady mass flux in that the far-infrared luminosity of HL Tau, $L_d = 6.7$ $L_\odot$, cannot be accounted for by reprocessing of stellar photons alone. HL Tau's flat temperature distribution of $T \sim r^{-1/2}$ (Beckwith et al. 1990) would also find natural explanation in a disk with a mass flux which is an increasing function of radius.

In addition to HL Tau, 14 of the 86 sources in Beckwith et al. (1990) survey are such that $L_d > L_*$. All of these sources (including DG Tau which is also a continuum source with a jet) have flat spectral energy distributions which can be modeled as mass infall rates of a few times 10^{-6} $M_\odot$ yr^{-1}, yet have small stellar luminosities (≈ 1 $L_\odot$) which (assuming neglected UV luminosities are small as suggested by Valenti et al. 1993) imply small stellar accretion rates. This contradiction can be resolved if mass is accumulating in the disks of these objects. In the absence of strong winds these disks must be periodically flushed, perhaps in FU Orionis–type outbursts, to prevent disk masses from quickly rising above observed values ($M_d < 0.1$ $M_\odot$). In this group, that one out of six sources is thought to be subject to FU Orionis outbursts suggests that the timescale for the FU Orionis phase is conservatively $\approx 1/10$ the average protostellar age of 10^6 yr or about 10^5 yr in duration (Kenyon et al. 1993b).

5. DISCUSSION

V1515 Cyg–type outbursts can be explained with a self-regulated, BL 94–type outburst. Infall from a circumstellar envelope naturally provides a mechanism to account for the apparent repetitiveness of the phenomenon. With constraints on the value of the viscous efficiency, timescales are found which are in reasonable agreement with observations. Explaining the more rapid risetimes of FU Ori and V1057 Cyg may require a perturbation or a different mass transport mechanism than herein investigated. In this section several implications of the thermal outburst model are discussed.

5.1. *Rapid Risetime Outbursts*

One of the notable things about the results of this limited parameter study is that for a given $\dot{M}_{\rm in}$, a range of perturbation parameters can lead to very similar light curve shapes (cf. models A1, A2, and A3). In a general way, outbursts fall into two categories: (1) inside-out outbursts for which the initiation of instability in the inner disk leads to slow risetimes (these include both self-regulated outbursts such as models B1 and B2 and disks perturbed too weakly to trigger outside-in outbursts like model B3) and (2) outside-in outbursts for which the initiation of instability near $R_{\rm limit}$ results in rapid risetimes. (This is an oversimplification; in fact the outbursts display a continuous range of behavior.) Some limits can be put on the type of perturbation which may lead to a rapid-risetime (outside-in) outburst. The mass of the perturbation may be small; for an $\dot{M}_{\rm in} = 5 \times 10^{-6}$ $M_\odot$ yr^{-1} disk, for example, a 5×10^{-3} $M_\odot$ perturbation can trigger a rapid-risetime outburst; for a 1×10^{-6} $M_\odot$ yr^{-1} disk, 10^{-3} $M_\odot$ is sufficient (Bell 1993). The value of $\Delta\Sigma/\Sigma$ primarily influences the peak magnitude but also slightly affects the timescale of decline from out-

burst (Fig. 5). The strongest constraint deduced from the models tested is that in order to trigger a rapid-risetime outburst in a supercritical disk, *the perturbation must occur at a radius less than* $R_{\rm limit}$ *or* $\lesssim 1/4$ AU.

Although there are two well-documented cases (FU Ori and V1057 Cyg), rapid-risetime outbursts may not, in fact, be very common. All of the other three Fuors with confirmed outbursts—Elias 1-12, V346 Nor, and RNO 1B—have light curves which are consistent with brightening over many years timescale. Outburst event statistics are very uncertain, and certainly there is some selection in favor of identifying fast eruptions. Also, selection is in favor of rapid risetime outbursts in that older, more exposed systems are expected to have disks with lower or even subcritical mass fluxes for which rapid-risetime outbursts are more common than in more deeply embedded, younger objects. It may be that rapid-risetime outbursts are in fact rare.

With the current numerical realization, perturbations are required to produce rapid-risetime outbursts. If the perturbation arises from the close passage of a binary star, some constraints can be put on its orbit. The companion must have a very small periastron distance ($r \lesssim 0.1$ AU), and a sufficiently large apoastron distance (perhaps 100s of AU) to avoid perturbing the disk more often than viscous evolution can replenish it. Such a highly eccentric orbit may not represent a bound system. The mass of the perturber must also be rather low to avoid destroying the disk. For a parabolic fly-by, for example, a perturber with mass greater than half the mass of the disk ($M_d \lesssim 0.1\ M_\odot$) would impact with energy equal to the binding energy of the disk and be likely to destroy it (Clarke & Pringle 1991). There are not many highly eccentric, extreme mass ratio binaries among solar-type field binaries (Duquennoy & Mayor 1991). In the early phases of low-mass stellar evolution binarity may have been more common than in present-day main-sequence stars (Ghez, Neugebauer, & Matthews 1993; Leinert et al. 1993), but it is by no means clear that such systems are common enough to explain observed FU Orionis statistics.

Because of the small masses required (as small as $10^{-4}\ M_\odot$ in some test cases) the disk may not require perturbation from a binary companion to trigger the rapid risetimes of FU Ori and V1057 Cyg. For supercritical disks, the lower $\dot{M}_{\rm in}$, the smaller the perturbation mass required to trigger an outside-in outburst, but the closer to the central object such perturbation must occur. For $\dot{M}_{\rm in}$ below the critical value, however, the inner disk temperature falls below the conditions required for the ionization for hydrogen, so the required perturbation mass again rises. The perturbation mass required is therefore smallest for disks accreting at the critical rate of $5 \times 10^{-7}\ M_\odot\ {\rm yr}^{-1}$. For some disks, clumpiness or boundary-layer feedback in the inner disk or the accretion of protoplanetary masses may be sufficient to explain rapid-risetime outbursts.

5.2. *Low-State Luminosities and SEDs*

The thermal instability model predicts relatively low luminosities of protostars most of the time. Even when infall at a few times $\times 10^{-6}\ M_\odot\ {\rm yr}^{-1}$ lands on the disk, most of this mass halts at $R_{\rm limit}$ in the low state. Thus, the total luminosities of these objects are in the $\sim 1\ L_\odot$ range, consistent with surveys of Class I sources in Taurus (Kenyon et al. 1993a; Beichman, Boulanger, & Moshir 1992), but inconsistent with models in which all of the infalling material immediately accretes down to the stellar radius (Fletcher & Stahler 1994).

As shown in § 4.5, a 3 μm peak is a robust prediction for the low state under the thermal instability model. Unfortunately, detection of such a peak is made difficult by surrounding dusty envelopes. If FU Ori outbursters are generally found in the earliest phases of stellar evolution, as suggested by their extinctions, and by the model necessity of having infalling material still landing on their outer disks, then the infalling envelopes will obscure the central object even at wavelengths $\lesssim 3$ μm, and the peak will not be detectable. In other words, the pre-outburst state could be a low-luminosity Class I source or protostar. The SEDs of such objects in Taurus show that most of the short-wavelength radiation from the central objects is extincted by dusty envelopes (Kenyon et al. 1993a, c). Distinguishing radiation from the disk from radiation from the infalling envelope might best be accomplished for objects observed nearly pole-on, where a bipolar flow might clear out the line of sight making the central object less obscured (cf. Kenyon et al. 1993c).

It may be that the necessity of a large infalling mass flux precludes observation of this spectral feature in most objects except in the brief time between the dissipation of the envelope and the draining of the disk below the critical mass flux. Nevertheless, surveys of the objects in Taurus do show a few low-mass objects which have bumps at 3 μm. These objects do not, however, show the large far-infared emission that would be predicted for an infalling envelope (Kenyon & Hartmann 1995) indicating perhaps that such infall is very weak or has recently ended. Again, observation of the 2.3 and 4.6 μm CO features in absorption would strengthen identification of an active disk in any candidate quiescent Fuor.

5.3. *Physical Mechanisms of Mass Transport*

Throughout both this work and Bell & Lin (1994) the details of the physical mechanism of mass transport have been ignored using instead the α prescription as a way of parameterizing our ignorance. One of the most surprising conclusions of this work is the particularly small magnitude of the parameter α required to match outburst timescales. This magnitude is sufficiently small as to create problems with timescales of evolution and with disk masses. Because $\tau_{\rm visc} \approx r^2/\nu$ (e.g., BL 94), with the low-state α of 10^{-4} and $H/r \approx 0.1$, it would take $\sim 5 \times 10^6$ yr to accrete matter from only 10 AU and 2×10^8 yr from 100 AU. Furthermore, because the mass of the disk is inversely related to α, $M_d \sim \Sigma \sim \nu^{-1}$, a small α would be expected to result in unacceptably large disk mass. Nevertheless, numerical studies have shown that this low value of α might be appropriate for a viscosity which taps into the turbulence generated by the convective instability (Cabot et al. 1987; Ruden, Papaloizou, & Lin 1988). Recent studies have shown that convection may be present over a large region of the disk but such models are only self-consistent in the *absence* of other strong sources of viscosity (Kley, Papaloizou, & Lin 1993; Różyczka, Bodenheimer, & Bell 1994). Kley et al. (1993) find self-consistent convection at 5 AU in a $10^{-8}\ M_\odot\ {\rm yr}^{-1}$ protostellar disk when the underlying α viscosity is $\alpha = 10^{-3}$ but not when $\alpha = 10^{-2}$.

Further, observational statistics from the Taurus cloud (Lin et al. 1994) suggest a much larger time-averaged α of ≈ 0.1 over most of the disk. With $\alpha = 10^{-1}$, matter from 100 AU can be accreted in the physically plausible time of 2×10^5 yr (approximately the lifetime of the embedded phase) and from 1000 AU in 5×10^6 yr (approximately the age of the oldest, optically thick disks). It may be that different mass transport

mechanisms operate in different regions of the protostellar disk, and that each mechanism may have very different efficiencies. In any given regime, whichever process provides the most efficient mass transport mechanism will provide the local viscosity.

It may be that gravitational instability is the dominant mechanism for mass transport in the outer disk (e.g., Lin & Pringle 1987). In the absence of external radiation, a gravitational instability maintains the local value of the Toomre Q_T parameter ($Q_T \equiv c_s \Omega/\pi G\Sigma$) approximately equal to one. If Q_T decreases below one, gravitational instability provides a local heat source which raises the value of Q_T. If Q_T increases above one, the local heat source is quenched, and the disk contracts and cools until the value of Q_T drops below one. In a disk for which $Q_T = 1$, analyses in BL 94 suggest that either $\dot{M}$ or α must be a strong function of radius. If α is held constant, then $\dot{M}$ must *decrease outwards* as $r^{-3/2}$. If mass is being added to the outer disk at an approximately constant rate, this situation is highly unstable. If instead mass flux is assumed to be constant with radius and α is allowed to vary, it can be shown that the effective α_{grav} for transport of mass due to gravitational instability increases outward such that

$$\alpha_{grav} = 0.1\left[\frac{\dot{M}(r)}{10^{-5}\, M_\odot\ \mathrm{yr}^{-1}}\right]\left(\frac{M_*}{M_\odot}\right)^{-3/2}\left(\frac{H/r}{0.1}\right)^{-3}\left(\frac{r}{30\ \mathrm{AU}}\right)^{3/2}. \quad (10)$$

For any source of viscosity *other than gravitational instability* to be the dominant mechanism of mass transfer, it must have an efficiency α_x greater than the above value of α_{grav}.

In a $10^{-5}\ M_\odot\ \mathrm{yr}^{-1}$ disk α_x must be greater than 10^{-3} at 1.5 AU to dominate over gravitational instability and greater than 10^{-4} at 0.3 AU. For a $10^{-6}\ M_\odot\ \mathrm{yr}^{-1}$ disk the corresponding radii are 6.5 and 1.4 AU, respectively. This derivation suggests that in the outer disk regions, gravitational instability may be the most efficient form of angular momentum transport, while in the inner disk where the gravitational instability is weak, some other source of viscosity such as convective turbulence may provide the dominant source of viscosity. In summary, we suggest that the effective viscous efficiency itself may be a strong function of radius in protostellar disks, so the large surface densities implied by our small value of α do not necessarily conflict with small observationally derived disk masses.

6. SUMMARY

In this contribution, a surface density perturbation has been added to the BL 94 thermal outburst models with which are explored a variety of possible outburst forms. We note the following features:

1. Disks for which $\dot{M}_{in} >$ the mass flux critical for outburst, $\dot{M}_{crit}$ ("supercritical" disks), spontaneously undergo periodic, self-regulated outbursts without the need for perturbation. Application of a perturbation in such systems may change the form of an already impending outburst.
2. Disks for which $\dot{M}_{in} < \dot{M}_{crit}$ ("subcritical" disks) require perturbation to undergo outburst; additional perturbation must be postulated to explain repeated outburst.
3. Self-regulated outbursts are generally initiated near the inner edge of the disk and result in a predominantly "inside-out" progression of the ionization front.
4. Triggered outbursts may be initiated anywhere in the disk (though are easiest to trigger for $r < R_{limit}$) and result in an "outside-in" progression of the primary ionization front. In a triggered outburst a secondary ionization front is also initiated which propagates outward from the ignition radius.
5. Outbursts evolve through two phases: an initial "spike" phase regulated by the propagation of the inward-moving ionization front and therefore sensitive to the details of the perturbation, followed by a longer "plateau" phase regulated by the propagation of the more general outward-moving front.
6. Decay timescales for all outbursts are governed by the slow movement of the outward-propagating front and are therefore long.

In addition we have "observed the models" and find the following general agreement with observations:

1. Models can be developed to match a wide variety of light curve shapes and magnitudes including reasonable fits to observations of *B* light curves for FU Ori, V1515 Cyg, and V1057 Cyg.
2. Both during outburst and during decay from peak light, magnitude changes are greater at optical wavelengths than in the infrared.
3. The lack of decline in luminosity in intermediate-wavelength bands ($\sim 5\ \mu$m) seen after peak light in V1057 Cyg is a natural consequence of this model in which the inner mass flux slowly decreases after peak light while the outer mass flux remains constant.
4. Because of the slow outward progression of the ionization front in both triggered and self-regulated outbursts, a decrease in line width after peak light is a natural consequence of the accretion-disk outburst model.
5. At wavelengths shorter than 1.5 μm, decay from outburst is expected to be preceded by an increase in line widths.
6. During outburst, spectral energy distributions (SEDs) are dominated at short wavelengths by radiation from the inner, high mass flux region. At longer wavelengths spectra are dominated by cooler radiation from outer, steady lower mass flux region.
7. In outbursting objects there will be a change of mass flux in the disk at a radius which is a small fraction of an AU ($\lesssim \frac{1}{4}$). In an outbursting object this will appear as an SED which is steeper than the best-fit constant mass flux SED in the 2–8 μm region.
8. If the transition radius occurs at 1/10 of an AU or less, the peak wavelength of the resulting SED will be significantly shifted to shorter wavelengths from the constant mass flux model. This effect will be most important in the earliest stages of outburst or in outbursts in low-mass flux disks and could cause maximum surface temperatures and inner accretion rates to be systematically overestimated.
9. Models further suggest that accretion rates derived from observed maximum surface temperatures could be slightly underestimated because of the effects of departure from vertical thermal balance during outburst.
10. During quiescence the constant mass flux outer region appears as a flat or rising spectrum source. The FU Orionis outburst phase is expected to be primarily confined to the embedded YSO phase at ages $\lesssim 10^5$ yr.

One of the major limitations of this model is its failure to consider the effects of surface irradiation (reprocessing) from either central object or inner accretion disk. Although, as discussed above, impact may be small on SEDs and light curves, this process may have dynamical consequences for the sustain-

ing of outburst timescales and for the propagation of the outward ionization front itself. Inclusion of this effect requires accounting for the constantly changing shape of the disk's surface as well as an estimate of boundary layer radiation during the quiescent phase.

We are grateful to Pat Cassen for many helpful discussions of the problems involved in this paper and for suggesting portions of the spectral energy distribution analysis. We also wish to acknowledge enlightening conversations with Peter Bodenheimer, Cathie Clarke, Dave Hollenbach, Burt Jones, and Willi Kley and helpful suggestions from the referee Steve Strom. K. R. B. would like to acknowledge support from a Sigma Xi award and from NASA training grant NGT-50665. Part of this work was conducted under the auspices of a special NASA astrophysics theory program that supports a Joint Center for Star Formation Studies at NASA Ames Research Center, the University of California at Berkeley, and the University of California at Santa Cruz and was also supported in part by NASA Origins grant NAGW-2306.

REFERENCES

Adams, F. C., Lada, C. J., & Shu, F. H. 1987, ApJ, 312, 788
Beckwith, S. V. W., Sargent, A. I., Chini, R. S., & Güsten, R. 1990, AJ, 99, 924
Beichman, C. A., Boulanger, F., & Moshir, M. 1992, ApJ, 385, 248
Bell, K. R. 1993, Ph.D. thesis, Univ. California, Santa Cruz
———. 1994, in The Nature and Evolutionary Status of the Herbig Ae/Be Stars, ed. P. S. Thè, M. P. Pèrez, & E. P. J. van den Heuvel (ASP Conf. Series 62), 215
Bell, K. R., & Lin, D. N. C. 1994, ApJ, 427, 987 (BL 94)
Bell, K. R., Lin, D. N. C., & Ruden, S. P. 1991, ApJ, 372, 633
Blondel, P. F. C., Talavera, A., & Tjin A Djie, H. R. E. 1993, A&A, 268, 624
Bonnell, I., & Bastien, P. 1992, ApJ, 401, L31
Cabot, W., Canuto, V. M., Hubickyj, O., & Pollack, J. B. 1987, Icarus, 69, 423
Calvet, N., Hartmann, L., Kenyon, S. J., & Whitney, B. A. 1994, ApJ, 434, 330
Carr, J. S. 1988, ApJ, 345, 522
Clarke, C. J., Lin, D. N. C., & Pringle, J. E. 1990, MNRAS, 242, 439
Clarke, C. J., & Pringle, J. E. 1991, MNRAS, 249, 584
Duquennoy, A., & Mayor, M. 1991, A&A, 248, 485
Fletcher, A. B., & Stahler, S. W. 1994, ApJ, 435, 313
Ghez, A. M., Neugebauer, G., & Matthews, K. 1993, AJ, 106, 2005
Goodrich, R. W. 1987, PASP, 99, 116
Gottlieb, E. W., & Liller, W. 1978, ApJ, 225, 488
Haro, G. 1972, Inf. Bull. Var. Stars, No. 714
Hartmann, L. W., & Kenyon, S. J. 1985, ApJ, 299, 462
———. 1987a, ApJ, 312, 243
———. 1987b, ApJ, 322, 393
Hartmann, L. W., Kenyon, S. J., & Hartigan, P. 1993, in Protostars and Planets III, ed. E. H. Levy & J. Lunine (Tucson: Univ. Arizona Press), 497
Hayashi, M., Ohashi, N., & Miyama, S. M. 1993, ApJ, 418, L71
Herbig, G. H. 1966, Vistas Astron., 18, 109
———. 1977, ApJ, 217, 693
———. 1989, in ESO Workshop on Low Mass Star Formation and Pre-Main Sequence Objects, ed. B. Reipurth (Garching: ESO), No. 33, 233
Hessman, F. V., Eislöffel, J., Mundt, R., Hartmann, L. W., Herbst, W., & Krautter, J. 1991, ApJ, 370, 384
Hillenbrand, L. A., Strom, S. E., Vrba, F. J., & Keene, J. 1992, ApJ, 397, 613
Kawazoe, E., & Mineshige, S. 1993, PASJ, 45, 715
Kenyon, S. J., Calvet, N., & Hartmann, L. W. 1993a, ApJ, 414, 676
Kenyon, S. J., Gomez, M., Marzke, R. O., & Hartmann, L. W. 1994, AJ, in press
Kenyon, S. J., & Hartmann, L. W. 1991, ApJ, 383, 664 (KH 91)
———. 1995, in preparation
Kenyon, S. J., Hartmann, L., Gomez, M., Carr, J. S., & Tokunaga, A. 1993b, AJ, 105, 1505
Kenyon, S. J., Hartmann, L. W., & Hewett, R. 1988, ApJ, 325, 231 (KHH 88)
Kenyon, S. J., Hartmann, L. W., & Kolotilov, E. A. 1991, PASP, 103, 1069 (KHK 91)
Kenyon, S. J., Whitney, B., Gomez, M., & Hartmann, L. W. 1993c, ApJ, 414, 773
Kley, W., Papaloizou, J. C. B., & Lin, D. N. C. 1993, ApJ, 416, 679
Leinert, Ch., Zinnecker, H., Weitzel, N., Christou, J., Ridgway, S. T., Jameson, R., Haas, M., & Lenzen, R. 1993, A&A, 278, 129
Lin, D. N. C., Hayashi, M., Bell, K. R., & Ohashi, N. 1994, ApJ, 435, 821
Lin, D. N. C., & Papaloizou, J. 1985, in Protostars and Planets II, ed. D. C. Black & S. Matthews (Tucson: Univ. Arizona Press), 981
Lin, D. N. C., Papaloizou, J., & Faulkner, J. 1985, MNRAS, 212, 105
Lin, D. N. C., & Pringle, J. 1987, MNRAS, 225, 607
Różyczka, M. N., Bodenheimer, P. H., & Bell, K. R. 1994, ApJ, 423, 736
Ruden, S. P., Papaloizou, J., & Lin, D. N. C. 1988, ApJ, 329, 739
Savage, B. D., & Mathis, J. S. 1979, ARA&A, 17, 73
Shakura, N. I., & Sunyaev, R. A. 1973, A&A, 24, 337
Shu, F. H., Adams, F. C., & Lizano, S. 1987, ARA&A, 25, 23
Simon, T., & Joyce, R. 1988, PASP, 100, 1549
Smak, J. 1984, PASP, 96, 5
Valenti, J. A., Basri, G., & Johns, C. M. 1993, AJ, 106, 2024
Welty, A. D., Strom, S. E., Strom, K. M., Hartmann, L. W., Kenyon, S. J., Grasdalen, G. L., & Stauffer, J. R. 1990, ApJ, 349, 328
Whitney, B., Clayton, G. C., Schulte-Ladbeck, R. E., Calvet, N., Hartmann, L. W., & Kenyon, S. J. 1993, ApJ, 417, 687